

THE MEASUREMENT OF SULFUR OXIDATION PRODUCTS AND THEIR ROLE  
IN HOMOGENEOUS NUCLEATION

NASA Grant No. NAG5-6383  
Georgia Tech Project No. G35-W91

Final Report

July 1, 1997 – June 30, 1999

Submitted to:

NASA Headquarters, Code YS  
300 E Street, SW  
Washington, DC 20546

Attn: Dr. Ghassem Asrar

Submitted by:

School of Earth and Atmospheric Sciences  
Georgia Institute of Technology  
Atlanta, GA 30332

Principal Investigator: Dr. F. L. Eisele

## Final Report

This project was originally the third year of a three year research grant which, because of administrative changes within NASA, was funded in two parts. The first two years of this grant were funded through NASA Grant No. NAGW 4692 and the final year was funded through NASA Grant No. NAG5-6383. The final year was also extended by an additional year through a no-cost extension. Scientifically, however, the present project is simply a continuation of the previous 2 years of investigation which are summarized in the Final Report from project NAGW 4692. Exploratory work from the first two years led to several successful measurements in the present grant period.

Both original areas of study continue to be investigated. An improved version of a transverse ion source was developed which uses selected ion chemical ionization mass spectrometry techniques inside of a particle nucleation flow tube. These new techniques are very unique, in that the chemical ionization is done inside of the flow tube rather than by having to remove the compounds and clusters of interest which are lost on first contact with any surfaces. The transverse source is also unique because it allows the ion reaction time to be varied over more than an order of magnitude, which in turn makes possible the separation of ion induced cluster growth from the charging of preexisting molecular clusters. As a result of combining these unique capabilities, the first ever measurements of prenucleation molecular clusters were performed. These clusters are the intermediate stage of growth in the gas-to-particle conversion process. This new technique provides a means of observing clusters containing 2, 3, 4, ... and up to about 8 sulfuric acid molecules, where the critical cluster size under these measurement conditions was about 4 or 5. Thus, the nucleation process can now be directly observed and even growth

beyond the critical cluster size can be investigated. The details of this investigation are discussed in a recently submitted paper, which is included as Appendix A.

Measurements of the diffusion coefficient of sulfuric acid and sulfuric acid clustered with a water molecule have also been performed. These provide an indirect measurement of the amount of water which is associated with a sulfuric acid molecule from 0.3 up to about 70% relative humidity. These measurements are also discussed in more detail in another recently submitted paper which is included as Appendix B. The empirical results discussed in both of these papers provide a critical test of present nucleation theories. They also provide new hope for resolving many of the huge discrepancies between field observation and model prediction of particle nucleation.

The second part of the research conducted under this project was directed towards the development of new chemical ionization techniques for measuring sulfur oxidation products. The DMSO molecule was one of the primary focuses of this effort. DMSO is an important product of DMS oxidation and its concentration/production rate and subsequent oxidation products help to control the amount of sulfur partitioned between particle nucleation, aerosol growth, and acidification of droplets/rainout. A chemical ionization technique was developed in which protonated ethanol was used as the reactant ion for measuring DMSO. This technique was not only developed and tested in the laboratory, but was also recently used to make some of the first real time aircraft measurements of DMSO as part of the NASA PEM-Tropics-B program. The technique was quite successful and able to measure DMSO down to the 1 ppt (part per trillion) level. While the data from this program are still being analyzed, some of the preliminary results are shown in Figure 1. Overall, this one year project has been highly successful

and has led to a variety of important new measurement techniques which will expand present research capabilities in both the field and laboratory.

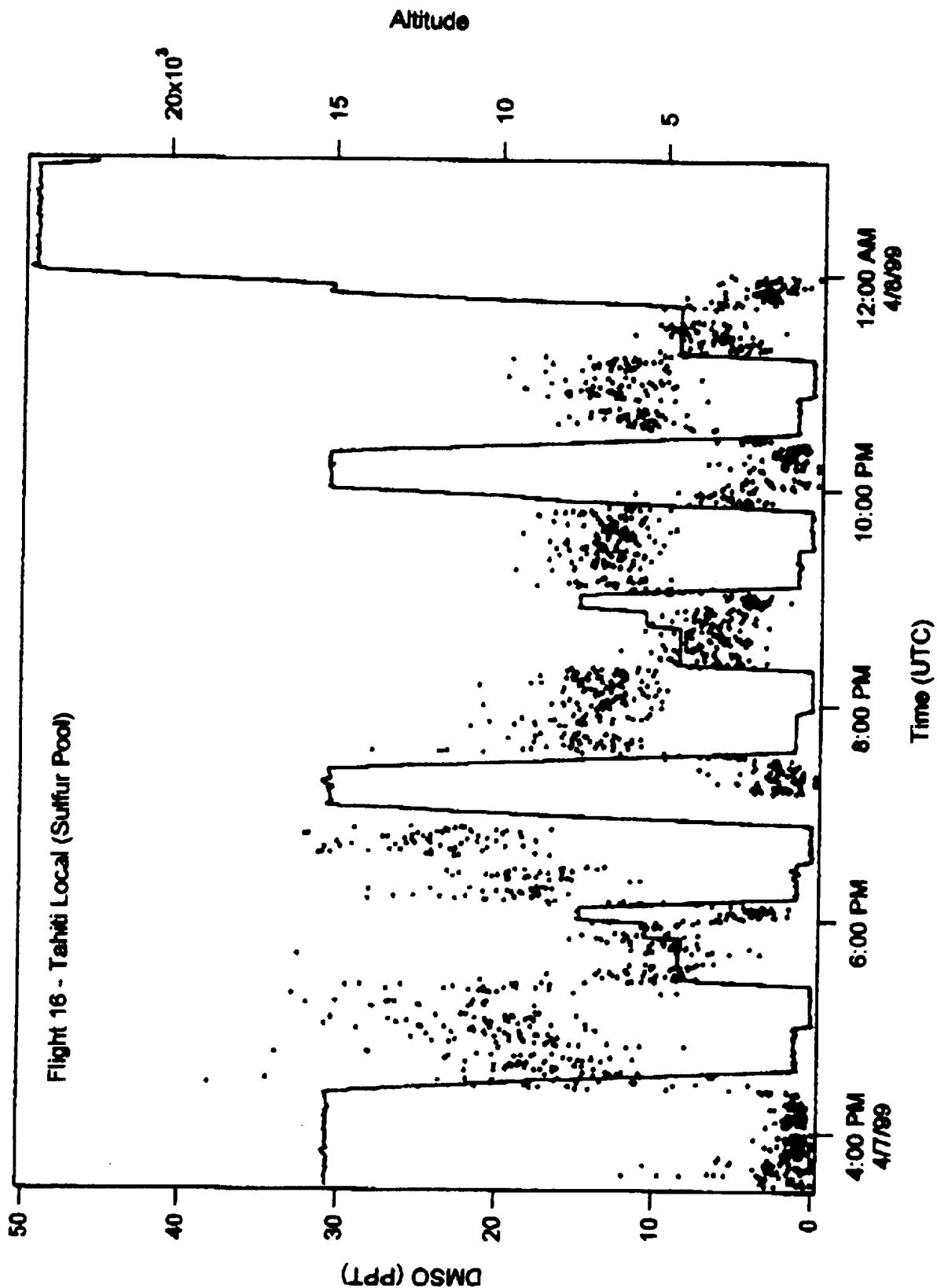


Figure 1. DMSO concentration (dots) plotted as a function of time during Flight 16 of PEM-Tropics B on the NASA P-3B aircraft. The solid line is the flight altitude. Note the dramatic increase in the boundary layer flight legs as expected.

# First Measurement of Prenucleation Molecular Clusters

F. L. Eisele<sup>#</sup> and D. R. Hanson

Atmospheric Chemistry Division, NCAR, Boulder, CO

23Aug99. For *J. Phys. Chem.*

## Abstract.

The molecular cluster ions  $\text{HSO}_4^-(\text{H}_2\text{SO}_4)_{n-1}$  corresponding to the neutral species  $(\text{H}_2\text{SO}_4)_n$  for  $n = 3$  to 8 have been observed using a transverse chemical ionization scheme located inside a cooled flow tube. The contribution of ion-molecule clustering reactions was ascertained and readily separated from the ionization of the neutral clusters. The presence of the clusters were strongly dependent on temperature and humidity. Ratios of successive clusters thought to be representative of steady-state are reported.

## Introduction.

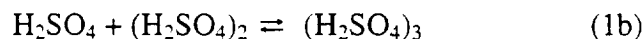
There is growing interest in atmospheric aerosols because of the large uncertainties in their influence on global radiative forcing, their potential health hazards in urban and industrial areas, and their largely unexplored role in tropospheric chemistry. Even the source terms for their production are not well understood. In general, particles enter the atmosphere in 3 ways: they are swept up off land or ocean surfaces, they are formed by gas-to-particle nucleation processes, and they are injected into the atmosphere via volcanoes and combustion processes (natural and anthropogenic). The first of these processes is largely controlled by nature but is influenced by humans through changing land use. The gas-to-particle nucleation process occurs

---

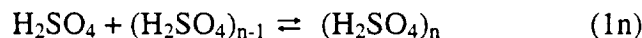
<sup>#</sup> also School of Earth and Atmospheric Sciences, Georgia Institute of Technology, Atlanta, GA 30332

naturally, but is highly non-linear and is easily influenced by anthropogenic emissions of gases such as SO<sub>2</sub>. The direct injection of particles into the atmosphere, for example, from forest fires, may involve a gas-to-particle nucleation process in the early stages. Aerosols that are injected into the atmosphere as a result of human activity often have their origin in some type of combustion process and are formed as a result of supersaturation/condensation of non-volatile exhaust gases. Thus, an improved understanding of the rather elusive gas-to-particle nucleation process is central to quantifying both natural particle production and anticipated increases in these production rates resulting from human activity.

The important first steps to at least a portion of new particle formation events in the atmosphere likely involve the sulfuric acid molecule, H<sub>2</sub>SO<sub>4</sub>.<sup>1</sup> For example, two H<sub>2</sub>SO<sub>4</sub> molecules may combine to give the H<sub>2</sub>SO<sub>4</sub> dimer, another H<sub>2</sub>SO<sub>4</sub> molecule may collide with the dimer resulting in a H<sub>2</sub>SO<sub>4</sub> trimer, etc. The equilibrium constants for the successive addition of H<sub>2</sub>SO<sub>4</sub> to these clusters



...



are  $K_2, K_3, \dots, K_n$ . There are other species in the atmosphere that may play a role in particle nucleation, notably H<sub>2</sub>O and NH<sub>3</sub>.<sup>2,3</sup> Theoretical treatments based on bulk liquid properties (classical hydrate theory)<sup>4,5</sup> indicate that hydration of H<sub>2</sub>SO<sub>4</sub> and its clusters could be extensive. For example, at 50 % relative humidity (RH), this theory predicts that the sulfuric acid monomer will be present primarily as H<sub>2</sub>SO<sub>4</sub>·H<sub>2</sub>O and H<sub>2</sub>SO<sub>4</sub>·(H<sub>2</sub>O)<sub>2</sub>. Therefore, reactions analogous to (1) but including hydration of (and possibly addition of NH<sub>3</sub> to) the products and reactants more properly describe equilibrium when these species are present.

Attempts to explain particle formation in the atmosphere have been handicapped by insufficient thermodynamic information for reactions such as (1). In many regions of the atmosphere<sup>1,2</sup> and for some laboratory results<sup>6-8</sup>, the rate of particle formation is not adequately explained by binary homogeneous nucleation in the H<sub>2</sub>SO<sub>4</sub>/H<sub>2</sub>O system using thermodynamics derived from bulk solutions. The atmospheric inadequacies of the binary theories have led researchers to propose that NH<sub>3</sub> plays a role in particle formation<sup>2</sup> and preliminary theory<sup>3</sup> and laboratory experiments<sup>6</sup> have demonstrated a pronounced effect on particle formation rates due to NH<sub>3</sub>. Furthermore, in laboratory measurements of the reaction of SO<sub>3</sub> with NH<sub>3</sub>, the dimer of sulfamic acid, (NH<sub>3</sub>SO<sub>3</sub>)<sub>2</sub>, and its cluster with H<sub>2</sub>SO<sub>4</sub>, NH<sub>3</sub>SO<sub>3</sub>H<sub>2</sub>SO<sub>4</sub>, were observed.<sup>9</sup> This demonstrated a potential role that NH<sub>3</sub> may have in particle formation and also showed that clusters of this type can be investigated using chemical ionization mass spectrometry.

This paper describes the measurement of molecular clusters of sulfuric acid under quiescent particle-growth conditions. It may be the first report of the detection of neutral H<sub>2</sub>SO<sub>4</sub> clusters. H<sub>2</sub>SO<sub>4</sub> clusters from the dimer up to clusters of 8 H<sub>2</sub>SO<sub>4</sub> molecules have been detected; the larger clusters being comparable to the critical cluster size found in laboratory experiments.<sup>6</sup> The measurements cover only a small range of concentration and cannot yet be directly applied to atmospheric nucleation calculations, however, the results provide a test for theory as well as reveal the power of the experimental technique. This technique provides a new window through which particle nucleation can be observed: each step of the process can now be studied. Finally, rough estimates of the steady state ratios of successive clusters are derived from the measured ion cluster distributions.

## Apparatus, and Measurement and Analysis Techniques

The measurement of  $\text{H}_2\text{SO}_4$  and its clusters were made in a thermostatted 9.5 cm ID flow tube using chemical ionization mass spectrometry (SCIMS). The SCIMS ion source and mass spectrometer inlet extend radially into the flow tube (3-to-6 and  $\sim 1$  cm, respectively, from the wall) to detect species *in situ*. The ion-molecule reaction time was usually varied by changing the voltage applied to the ion-source; the distance between source and inlet could also be varied. A variable ion-molecule reaction time provided a means to distinguish between ionization of neutral  $\text{H}_2\text{SO}_4$  clusters and ion-molecule clusters produced by stepwise addition of  $\text{H}_2\text{SO}_4$  molecules to  $\text{HSO}_4^-$  ions. The  $\text{H}_2\text{SO}_4$  concentration was kept low ( $\sim 2 \times 10^9 \text{ cm}^{-3}$ ) to minimize ion-molecule clustering while the flow tube temperature,  $T_c$ , was held at  $\sim 240$  K to induce formation of neutral clusters of  $\text{H}_2\text{SO}_4$ .

A schematic of the apparatus is presented in Figure 1. Flows containing  $\text{H}_2\text{SO}_4$  in  $\text{N}_2$  and  $\text{H}_2\text{O}$  in  $\text{N}_2$  were mixed at 298 K and  $\sim 620$  Torr (slightly above local ambient pressure) in a 5-cm ID  $\times$  25 cm long region at the top of the flow tube. At the end of an adaptor (5 cm ID to 9.5 cm ID) is located a cooled aluminum shower head assembly (0.64 cm inch thick with  $\sim 150$  holes 0.3 cm in diameter) that both collimates the flow and cools it to approximately  $T_c + 12$  K. Contact with the surfaces of the shower head results in about a factor of 2 loss of  $\text{H}_2\text{SO}_4$ . Once in the main flow tube (the temperature regulated section is  $\sim 65$  cm long and  $255 \text{ K} \leq T_c \leq 234$  K), the gas mixture cools further to about 2-to-5 K over  $T_c$  while it travels the 25-to-40 cm distance to the measurement region, where the ion source and inlet are located. The total  $\text{N}_2$  flow rate was 10-12 STP liter  $\text{min}^{-1}$  resulting in an average flow velocity of  $\sim 2.5 \text{ cm s}^{-1}$  thus a time period of 10-to-15 s was allowed for the gas to cool further and for  $\text{H}_2\text{SO}_4$  to form clusters.  $\text{H}_2\text{SO}_4$  and its clusters were ionized with  $\text{NO}_3^-$  core reactant ions as they passed between the ion

source and mass spectrometer. The ions were prepared by flowing a dilute  $\text{HNO}_3$ -in- $\text{N}_2$  gas mixture through the ion source (a 0.64 cm ID  $\times$  2 cm long tube containing radioactive  $^{241}\text{Am}$ .) The exit of the source is fitted with a 3 cm  $\times$  3 cm plate (0.2 mm thick) that had a 0.7 cm hole in the center which the ions pass through. The distance between the ion source and mass spectrometer entrance port (100  $\mu\text{m}$  diameter hole) was generally 4 cm but was varied between 2.5 and 6 cm.

A collisional-dissociation chamber (CDC) is located just after the 100  $\mu\text{m}$  entrance orifice where core ions can be stripped of associating species such as  $\text{HNO}_3$  before entering the differentially pumped mass spectrometer. In its typical application, the CDC is at a pressure of  $\sim$  0.1 torr, and the application of an electric field of  $\sim$ 10 V/cm will strip most ions of associating species.<sup>10</sup> Here, the electric field was kept small,  $\sim$  0.2 to 2 V/cm, just enough to give an adequate transmission of ions through the CDC region. There was no evidence for breakup of  $\text{HSO}_4^-(\text{H}_2\text{SO}_4)_{n-1}$  clusters as the CDC electric field was varied over this range although the amount of  $\text{HNO}_3$  attached to the ions was observed to vary.

Ionization of  $\text{H}_2\text{SO}_4$  occurs as the  $\text{NO}_3^-$  and  $(\text{HNO}_3)_m\text{NO}_3^-$  reactant ions (the majority of reactant ions are  $m=1$ , hereafter the reactant ions are referred to in short as  $\text{NO}_3^-$  ions) traverse the central portion of the flow tube following the electric field lines which terminate at the entrance aperture to the mass spectrometer. The drift time of an ion is determined by its mobility, the electric field strength, and the distance it must travel. The ion source voltage was varied from  $-400$  to  $-5000$  V resulting in drift times of  $\sim$  40 to 4 ms for a mobility of  $\sim$ 1.5  $\text{cm}^2/\text{sV}$  and a typical distance of 4 cm. This approximate drift time is the time for reaction of  $\text{NO}_3^-$  with  $\text{H}_2\text{SO}_4$  and with the  $(\text{H}_2\text{SO}_4)_n$  molecular clusters under study. Also during this time  $\text{H}_2\text{SO}_4$  vapor will cluster with the  $\text{HSO}_4^-$  product ions (ion-induced cluster growth) leading to the

identical ions as produced in the ionization of neutral clusters. Ion clusters such as  $\text{HSO}_4^-(\text{H}_2\text{SO}_4)_n$  are strongly bound and their rate of formation from  $\text{H}_2\text{SO}_4 + \text{HSO}_4^-(\text{H}_2\text{SO}_4)_{n-1}$  are likely to be fast. It is assumed that both processes are contributing to the ions being observed and they are discussed in detail below.

The ion signals for the clusters were affected by mass discrimination within the instrument, notably the mass resolution of the quadrupole. For high mass resolutions such as a  $\Delta m/m$  of  $\sim 1$  (FWHM) at 500 amu (see the inset in Figure 3), high mass ions were suppressed, e.g., the signal due to the hexamer was usually not observable. For low resolution settings, however, such as  $\Delta m/m \sim 10$  at 500 amu (main part of Figure 3), many high mass ions were observed. For low resolution, the ratio of successive clusters was observed to be relatively insensitive to mass resolution for clusters up to  $n = 6$ . Shown in Figure 2 is a plot of the ratios for the  $n$ th cluster /  $(n-1)$ th cluster as a function of mass resolution setting. This setting primarily affects the mass resolution for high masses,  $> 200$  amu. Note that decreasing the resolution of the instrument may cause neighboring peaks to overlap/interfere with the ones we are interested in, and this may be responsible for the variation in some of the ratios at low settings. Nonetheless, it is evident that most of the changes in these ratios occur at high mass resolutions; the ratios of cluster signals are reported for low mass resolution (setting = 4.0) or corrected to these values using this plot. Other processes influencing mass discrimination, e.g., the lenses and detector/multiplier voltages, are likely to have only small effects on the ratios of successive clusters.

The temperature of the gas in the flow tube during these initial studies was not uniform owing to the large cooling that must occur. The gas temperature a few cm from the flow tube wall was measured with a thermocouple probe. The aluminum shower head cools the gas from

298 K to a temperature of  $\sim T_c + 12$  K while it and the flow tube are at  $T_c$ . The gas cools to a temperature of  $\sim T_c + 5$  K at a position of 25 cm into the flow tube (from the top) and to  $T_{\text{gas}} \sim T_c + 2$  K after 40 cm of travel into the flow tube. These were the two positions of the ion detection region. The data presented here was generally taken at the 40 cm distance because of the longer residence time and the more uniform temperature (gradient,  $\Delta T/\Delta z$ , was  $\sim 0.3$  K/cm whereas at 25 cm  $\Delta T/\Delta z \sim 0.5$  K/cm.) However, comparisons with data from the 25 cm distance are also discussed. Despite the non-uniform temperature of the gas, the distributions determined from the signal ratios for some of the clusters could be representative of steady state values.

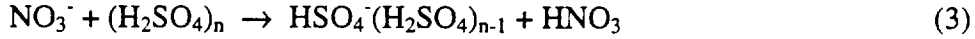
How well the measurements reflect the steady-state distributions of the clusters is dependent on how fast each cluster equilibrates. If the forward rate coefficients for (1) are close to the collision rate and the dissociation rates are fast (comparable to or faster than the pseudo-first-order forward reaction rate coefficients), our measurements may reflect steady-state or even equilibrium distributions. Results for the 25 cm and 40 cm distances (i.e., different neutral reaction times) are comparable and suggest that these assumptions are valid at least for the smaller clusters ( $n=2-4$ ). Determining equilibrium constants from the measured distributions requires a more stringent criteria, e.g., the loss rate of the  $n$ th cluster to form the  $(n+1)$  cluster, due to addition of  $\text{H}_2\text{SO}_4$ , must be much less than  $n$ th cluster's decomposition rate. If the  $n$ th cluster lies in the vicinity of the critical cluster, a dynamical model and accurate time information would be required to extract equilibrium constants.

### **Ion processes**

In the case of direct proton exchange between  $\text{NO}_3^-$  and pre-existing neutral clusters, the rates of ion formation are given by:



for the monomer (which has a rate coefficient  $k_1$ ) and for the  $n$ th cluster:

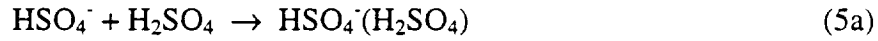


with a rate coefficient,  $k_n$ . Thus the incremental production of  $\text{HSO}_4^-(\text{H}_2\text{SO}_4)_{n-1}$  in time  $dt$  from neutral cluster  $(\text{H}_2\text{SO}_4)_n$  is approximately equal to:

$$[\text{NO}_3^-][(\text{H}_2\text{SO}_4)_n]k_n dt \quad (4)$$

If it can be assumed that only small decreases in  $[\text{NO}_3^-]$  occur by all ion-molecule reactions,  $dt$  can be replaced by  $t$ , the ion drift time for  $\text{NO}_3^-$ .

In the case of successive  $\text{H}_2\text{SO}_4$  incorporation onto the  $\text{HSO}_4^-$  ions formed in (2), the following series of reactions may occur:



...



The rate coefficient for (5a) is designated  $k'_2$  and, similarly, the rate coefficient for (5b) is designated  $k'_n$ . The instantaneous production rate at time  $\tau$  of the cluster with  $n$  sulfuric acid species in it is given by

$$[\text{H}_2\text{SO}_4][\text{HSO}_4^-(\text{H}_2\text{SO}_4)_{n-2}](\tau)k'_n d\tau \quad (6)$$

where  $[X](\tau)$  indicates the concentration of  $X$  at time  $\tau$ . Likewise, the production rate for the  $\text{HSO}_4^-(\text{H}_2\text{SO}_4)_{n-2}$  ion is given by

$$[\text{H}_2\text{SO}_4][\text{HSO}_4^-(\text{H}_2\text{SO}_4)_{n-3}](\tau)k'_{n-1} d\tau \quad (7)$$

Starting with (2) and successively integrating (over  $\tau$ ) these up to the  $n$ th cluster, the [ $n$ th ion cluster] is given by

$$[\text{NO}_3^-][\text{H}_2\text{SO}_4]^n k_1 k'_2 \dots k'_n \frac{t^n}{n!} \quad (8)$$

assuming that the decreases in ion concentrations due to reaction with  $\text{H}_2\text{SO}_4$  are small,  $[\text{H}_2\text{SO}_4]$  is constant, and the mobility of the ion is independent of  $n$ .<sup>12</sup> Note that the values of  $k_n$  and  $k'_n$  rate coefficients are likely to be similar and also close to the effective ion collision rate, i.e., on the order of  $10^{-9} \text{ cm}^3 \text{ s}^{-1}$ .

The chemistry detailed above has been presented in a simplified manner. In the flow tube apparatus, for example, the  $\text{NO}_3^-$  and  $\text{HSO}_4^-$  ions are present primarily as cluster ions with a single  $\text{HNO}_3$  molecule. These ions, as well as  $\text{H}_2\text{SO}_4$  itself,<sup>4</sup> may have  $\text{H}_2\text{O}$  molecules clustered with them. Treating these species as if they had no  $\text{HNO}_3$  and  $\text{H}_2\text{O}$  molecules associated with them is acceptable because most, if not all, of the reactant ion clusters probably undergo similar reaction with  $\text{H}_2\text{SO}_4$  and its hydrates as do the core ions (even the rate coefficients are similar).<sup>10,11</sup> We assume that the subsequent reactions, (3) and (5), are similarly unaffected by the presence of  $\text{HNO}_3$  or  $\text{H}_2\text{O}$ . The ion processes are treated separately above. In the experiment, they are occurring simultaneously and sometimes at comparable rates. For example, a neutral cluster that is ionized by  $\text{NO}_3^-$  may add an additional  $\text{H}_2\text{SO}_4$  molecule during its traverse to the SCIMS inlet. Also, ion cluster + neutral cluster reactions, for example, consider (3) or (5) with  $\text{H}_2\text{SO}_4$  replaced by  $(\text{H}_2\text{SO}_4)_m$ , are negligible because  $[(\text{H}_2\text{SO}_4)_m] \lll [\text{H}_2\text{SO}_4]$ .

The principal difference between these two schemes, ionization of a pre-existing neutral cluster versus product ion clustering with  $\text{H}_2\text{SO}_4$ , is their dependence on time. The production of ions from the  $(\text{H}_2\text{SO}_4)_n$  neutral clusters has a linear time dependence for all  $n$ ; thus, the ratio of any two of the ions produced from neutral clusters would be independent of ion reaction time. On the other hand, the  $\text{HSO}_4^-(\text{H}_2\text{SO}_4)_{n-1}$  product of ion induced clustering depends on time to the

$n$ th power and the ratio of any two ion clusters would have a dependence on time equal to the difference in the number of  $\text{H}_2\text{SO}_4$  molecules in the clusters. Therefore, the ion drift time dependence of the signals can be used to distinguish between neutral clusters and ion-induced clusters. By going to short reaction times and low  $[\text{H}_2\text{SO}_4]$  such that ion induced clustering is suppressed, particularly in the production of large clusters, the observed ions can be attributed to the ionization of neutral clusters.

Further evidence for detection of neutral clusters can be obtained by calculating the expected signal levels due to ion-clustering processes and comparing to the observed signals. For ions due solely to successive addition of  $\text{H}_2\text{SO}_4$  to  $\text{HSO}_4^-$ , the ratio of the ion cluster containing, for example, 5  $\text{H}_2\text{SO}_4$  moieties to that containing 1 is approximately given by  $([\text{H}_2\text{SO}_4] t k_1)^4 / 5!$ . For illustration,  $t$  and  $k'_n$  are assumed independent of  $n$  (see note 12.) With  $[\text{H}_2\text{SO}_4] = 3 \times 10^9 \text{ cm}^{-3}$ , an ion drift time  $t = 10 \text{ ms}$  and  $k'_n = 10^{-9} \text{ cm}^3 \text{ s}^{-1}$ , ion-cluster growth from (8) would give a value of  $\sim 10^{-8}$  for this ratio. If the observations of this ratio are much larger than this, as our results are, it indicates a detection of the neutral cluster. Also, the ion clustering reactions are relatively insensitive to temperature and the presence of water vapor. If the measurements show strong dependencies on these two parameters, this would also indicate the detection of neutral clusters as opposed to ion clustering.

### **Neutral clustering processes**

In order for the levels of neutral molecular clusters to be high enough to detect, there must be sufficient time available for these clusters to form in the flow tube. As mentioned above this time is  $\sim 10 \text{ s}$  (depending upon how cold the gas must be) or about  $10^3$  times longer than the ion-molecule reaction time. These neutral clusters are formed through a sequence of reactions as

depicted above in (1). Analogous to the sequential ion clustering scheme, where it is assumed that  $[\text{H}_2\text{SO}_4]$  is constant over time  $t$ , that any cluster formed is not significantly depleted by the formation of a larger cluster, and there is negligible decomposition of the clusters, the concentration of  $(\text{H}_2\text{SO}_4)_n$  can be taken to be equal to  $[\text{H}_2\text{SO}_4]^n t^{n-1} k_{2f} k_{3f} \dots k_{nf} / (n-1)!$  where  $k_{2f}, \dots, k_{nf}$  are the forward rate coefficients for (1a) to (1n), respectively. This is undoubtedly a simplification of the neutral system, the last assumption being particularly objectionable, however, this discussion is only for illustrative purposes. Again, using the example of the ratio of clusters containing 5 sulfuric acid molecules to those containing 1 molecule and for  $[\text{H}_2\text{SO}_4] = 3 \times 10^9 \text{ cm}^{-3}$ ,  $t = 0.7 \text{ s}$ , and  $k_{nf} = 1 \times 10^{-10} \text{ cm}^3 \text{ s}^{-1}$ , a ratio of  $\sim 10^{-4}$  for  $[(\text{H}_2\text{SO}_4)_5]/[\text{H}_2\text{SO}_4]$  could be attained if unbridled coagulation occurs. This is clearly not a rigorous calculation but illustrates that if  $\text{H}_2\text{SO}_4$  molecules react to form clusters at the gas-phase collision rate, a reasonable assumption, then a reaction time of as little as one second may be enough to allow for their presence at high enough levels that they can be observed (i.e., separated from ion clustering processes).

## Results and Interpretation

Shown in Figure 3 is a mass spectrum taken at low resolution ( $\Delta m/m \sim 10$  at 500 amu) with an ion-reaction time of  $\sim 25 \text{ ms}$ , 0.12 torr of water vapor, and gas temperature was  $-37 \text{ C}$  (236 K). Shaded in gray are masses associated with the initial core reactant ion  $\text{NO}_3^-$ : typically present as  $\text{NO}_3^-$  (62 amu) and as nitric acid clusters  $\text{NO}_3^- \cdot \text{HNO}_3$  (125 amu), and  $\text{NO}_3^- \cdot (\text{HNO}_3)_2$  (188 amu). Ions associated with sulfuric acid are indicated by filled triangles. Individual sulfuric acid molecules are observed as  $\text{HSO}_4^-$  (97 amu),  $\text{HSO}_4^- \cdot \text{HNO}_3$  (160 amu), and  $\text{HSO}_4^- \cdot (\text{HNO}_3)_2$  (223 amu) while the first sulfuric acid cluster is measured as the sum of  $\text{HSO}_4^- \cdot \text{H}_2\text{SO}_4$

(195 amu) and  $\text{HSO}_4^- \cdot \text{H}_2\text{SO}_4 \cdot \text{HNO}_3$  (258 amu). Successive sulfuric clusters  $(\text{H}_2\text{SO}_4)_n$  are observed as  $\text{HSO}_4^- \cdot (\text{H}_2\text{SO}_4)_{n-1}$  (293, 391, 489, 587, 685, and 783 amu). Sulfuric clusters of three or more were not generally observed to cluster with  $\text{HNO}_3$  (< 1 Hz net signal). A high resolution scan is included in the inset to show the 34 to 32 sulfur isotopes for the 391 and 489 peaks. They are in the proper ratios and helped to confirm the sulfate ion cluster peaks.<sup>13</sup> Note the absence of detection of any clusters containing  $\text{H}_2\text{O}$  molecules.

The lack of observed  $\text{H}_2\text{O}$  clustering on the nitric and sulfuric acid ions is probably due to the likely rapid loss of  $\text{H}_2\text{O}$  molecules from the ions. First, the ions may retain less water than the neutrals. Second, any  $\text{H}_2\text{O}$  associated with an ion may be driven off as the ion is sampled through the CDC (held at ~ 0.1 torr  $\text{N}_2$  and field strength of ~ 0.2 V / cm.) Water is far more volatile than sulfuric acid, and it likely re-equilibrates with clusters much more quickly than  $\text{H}_2\text{SO}_4$  does (i.e., fast rates for loss of  $\text{H}_2\text{O}$ .) Furthermore, the  $\text{H}_2\text{SO}_4$  ion cluster distribution did not vary with applied field in the CDC up to field strengths of a few V/cm. Thus,  $\text{H}_2\text{O}$ , but probably not  $\text{H}_2\text{SO}_4$ , can be lost during the ion's brief transit through this dry  $\text{N}_2$  gas. Thus, while the effects of  $\text{H}_2\text{O}$  on sulfuric acid cluster growth could be studied, the equilibrium water content of the clusters could not be directly observed.

As mentioned,  $\text{NO}_3^-$  denotes the sum of  $\text{NO}_3^-$  core ions (i.e.,  $\text{NO}_3^-$  + the nitric acid clusters listed above.) Also we use the terminology monomers, dimers, trimers etc. to refer to the total number of sulfuric acid molecules plus  $\text{HSO}_4^-$  core ions contained in an observed ion cluster, irrespective of the presence of  $\text{HNO}_3$  molecules. Since  $\text{NO}_3^-$  and its first two nitric acid clusters all react with  $\text{H}_2\text{SO}_4$  at about the ion collision rate ( $2 \times 10^{-9} \text{ cm}^3/\text{s}$  at 298 K)<sup>10,11</sup>, a rough estimate of  $\text{H}_2\text{SO}_4$  concentration can be obtained from  $(1/k_1t) \ln([\text{HSO}_4^-]/[\text{NO}_3^-] + 1) \cong (1/k_1t)[\text{HSO}_4^-]/[\text{NO}_3^-]$  where the bracketed quantities are the signals for those ions. We use a

value of  $1.5 \times 10^{-9} \text{ cm}^3 \text{ s}^{-1}$  for  $k_1$  at the measurement temperature of  $\sim 240 \text{ K}$ . It is not known how the  $\text{NO}_3^-$  clusters react with the neutral sulfuric acid clusters, and we assume that the clusters are ionized with equal efficiency.<sup>11</sup>

Figure 4a shows a plot of  $\ln([\text{HSO}_4^-]/[\text{NO}_3^-] + 1)$  as a function of ion drift time for water partial pressures of 0.12 and 0.04 torr at  $\sim 236 \text{ K}$ . Ion drift time was set by varying the voltage on the ion source while maintaining a constant source-inlet distance of 4 cm. Since the ordinate should be equal to  $k_1 t [\text{H}_2\text{SO}_4]$  a linear time dependence is expected and  $[\text{H}_2\text{SO}_4]$  is estimated to be  $1.2$  and  $2.4 \times 10^9 \text{ molecule cm}^{-3}$ , respectively. Linear regressions are also shown and a non-zero intercept is exhibited. This is probably due to the fact that the field lines are not parallel because there are no guard rings in the flow tube and the sampling of the ions may vary with the applied potential due to space-charge or other effects. It is also likely that  $\text{H}_2\text{SO}_4$  is not evenly distributed in the gas and thus different amounts of  $\text{H}_2\text{SO}_4$  could be sampled along the field lines.

The  $[\text{H}_2\text{SO}_4]$  for the high RH conditions was also measured by varying the source-inlet gap and results are shown in Fig. 4a as the shaded triangles. The gap distance was varied from 2.5 to 5.7 cm while maintaining a constant electric field strength. These results are in good agreement with the filled circle data and bolster our confidence in the experimental technique. It is evident, however, that when the distance exceeds  $\sim 5 \text{ cm}$  the estimation of  $[\text{H}_2\text{SO}_4]$  becomes increasingly worse. This could be due to the gap becoming much greater than the sizes of the ion source exit plate ( $\sim 3 \text{ cm}$ ) and inlet face plate ( $\sim 2 \text{ cm}$ ) thus allowing for increasingly divergent electric field lines. Finally, the signals for the  $n=2$  to 5 clusters were nearly identical to those presented below obtained by varying source voltage at constant source-inlet gap.

Figure 4b-d show the ratios of successive ion clusters of  $\text{H}_2\text{SO}_4$  to that of the monomer. From the previous section, a time dependence is expected for any such ratio if the ion cluster is due to successive  $\text{H}_2\text{SO}_4$  monomer addition to  $\text{HSO}_4^-$  ions, and this is clearly exhibited for the dimer (linear) and for the trimer (quadratic) when the relative humidity is low,  $\sim 20\%$  RH.<sup>14</sup> On the other hand, the ion clusters derived from a proton exchange between  $\text{NO}_3^-$  and a pre-existing neutral cluster should be time independent and this is clearly evident for the  $\text{HSO}_4^-(\text{H}_2\text{SO}_4)_{n-1}$  clusters for  $n \geq 3$  at 63% RH and for  $n \geq 4$  at 20% RH. Further evidence for the detection of the neutral clusters is exhibited in the magnitudes of the signals for the trimer and higher clusters at high RH versus those at low RH. The signals at low RH can be taken to be an upper limit to the effect of ion-induced clustering at high RH (indeed  $[\text{H}_2\text{SO}_4]$  is lower at high RH) assuming no water dependence for this process. Thus the observed signals cannot be due to ion clustering processes and are attributed to the presence of the neutral clusters  $(\text{H}_2\text{SO}_4)_3$ ,  $(\text{H}_2\text{SO}_4)_4$  and  $(\text{H}_2\text{SO}_4)_5$ .

The effect of temperature on the ion signals is shown in Figure 5, a semi-logarithmic plot of  $[\text{HSO}_4^-(\text{H}_2\text{SO}_4)_{n-1}] / [\text{NO}_3^-]$  versus  $1/T$ . Ion drift time was  $\sim 27$  ms and water vapor was constant at  $\sim 0.1$  torr and a resolution of  $\Delta m/m = \sim 1$  at 500 amu was set for the mass spectrometer. The signal due to the monomer is relatively constant as the temperature was lowered, and the dimer signal changed only slightly (increased losses of  $\text{H}_2\text{SO}_4$  due to temperature dependent eddies in the flow may be responsible for these changes), while the signals due to the  $n = 3$  and especially the  $n = 4$  and 5  $\text{H}_2\text{SO}_4$  clusters show substantial increases.

If a signal is due only to the ionization of a pre-existing neutral species, then the quantity plotted on the Y-axis can be related to the concentration of the neutral species. To the right of the plot is an alternative Y-axis that indicates [neutral] assuming a rate coefficient of

$1.5 \times 10^{-9} \text{ cm}^3 \text{ s}^{-1}$ , a reaction time of 27 ms and negligible mass discrimination. This axis probably does not apply to the dimer signal because it is primarily due to the ion clustering reaction.

Assuming a negligible contribution from the neutral dimer, the ratio of the dimer to the monomer signals of 0.025 results in a value for  $k'_2$  of  $1 \times 10^{-9} \text{ cm}^3 \text{ s}^{-1}$  for  $\text{HSO}_4^- + \text{H}_2\text{SO}_4$  using  $[\text{H}_2\text{SO}_4] = 1.8 \times 10^9 \text{ cm}^{-3}$  (the mobilities of  $\text{NO}_3^-$  and  $\text{HSO}_4^-$  are likely to be similar thus the  $2!$  term in (8) is accurate for  $n = 2$ .) This is a reasonable value and indicates that the dimer ion signal ( $n=2$ ) is primarily due to the ion molecule clustering reactions. Likewise, the trimer-to-dimer ion signal ratio at the warmest temperature is  $\sim 0.025$ , suggesting the  $n=3$  ion signal at this temperature may be due primarily to ion clustering reactions with  $k'_3 \sim k'_2$ .<sup>12</sup> As the temperature was lowered, however, the  $n=3$  signal due to the trimer neutral cluster appears. Especially notable are the  $n=4$  and 5 cluster signals which show strong temperature dependencies and are likely due to the increasing stability of the neutral clusters  $(\text{H}_2\text{SO}_4)_4$  and  $(\text{H}_2\text{SO}_4)_5$  as the temperature is lowered. Because of the mass resolution setting for this experiment ( $\Delta m/m = 1$  at 500 amu), the high-mass ions are discriminated against with respect to  $[\text{NO}_3^-]$  (on the order of factors of 3 and 9, respectively). Taking this into account, the concentration of the  $n = 4$  and 5 clusters is on the order of  $10^6$  to  $10^7 \text{ cm}^{-3}$  at the coldest temperature.

The ratio of  $(\text{H}_2\text{SO}_4)_5$  to  $(\text{H}_2\text{SO}_4)_4$  decreases slightly as the temperature is lowered and this indicates that the  $(\text{H}_2\text{SO}_4)_5$  cluster is not in equilibrium at least at the lower temperatures. Assuming the addition of  $\text{H}_2\text{SO}_4$  to the 4<sup>th</sup> cluster is exothermic by 10-to-15 kcal mol<sup>-1</sup>, the equilibrium ratio should increase by a factor of two to three as the temperature is decreased (the slight decrease in  $[\text{H}_2\text{SO}_4]$  was taken into account). This observation may indicate the lifetime of the 5<sup>th</sup> cluster may be longer than the growth time at  $\sim 236 \text{ K}$  (a few seconds). It also may indicate that growth out of this cluster to  $n = 6$  is faster than its decomposition rate and a steady-

state may have been approached. If this is true, the critical cluster for these conditions is less than  $n = 5$ , perhaps  $(\text{H}_2\text{SO}_4)_4$ .

Other observations indicate that the  $n = 5$  and higher clusters have not reached equilibrium or steady state at the low temperatures. Data taken at  $\sim 50\%$  RH at 257 K indicate a higher pentamer to tetramer ratio than the low temperature ( $\sim 240\text{K}$ ) data which indicates that equilibrium for the 5<sup>th</sup> cluster was not attained at  $\sim 240$  K. Also, data taken for comparable conditions at the two different neutral growth times (i.e., 25 and 40 cm) indicate that the pentamer (and to a lesser extent the tetramer) signal was larger for longer times. For this and larger clusters at  $T \leq 243$  K therefore, the time to achieve steady-state/equilibrium is likely comparable to the time that  $T_{\text{gas}}$  is within a few K of  $T_c$ , i.e., a few seconds. Note also that this time is comparable to the inverse of the pseudo-first order rate constant for formation of the  $n$ th cluster from the  $(n-1)$ th cluster ( $\sim 0.2 \text{ s}^{-1}$ ), assuming  $k_{\text{nf}} \sim 10^{-10} \text{ cm}^3 \text{ s}^{-1}$ .

Cluster distributions can be derived from the ratio of the ion signals due to the clusters. Because the ion signals for small clusters (notably,  $n=2$ ) were significantly affected by ion clustering processes, the ratios of the 195 and 293 amu signals to the monomer signal, such as shown in Fig. 4b and c, were extrapolated to zero ion time to get cluster/monomer ratios. Shown in Table 1 are the observed cluster ratios for the data shown in Figs. 3 and 4 and the 257 K data mentioned above. The data shown in Figure 5 is not included because it was taken at high mass resolution (thus the larger clusters were not observed) and also because the ion drift time was not varied.  $R_n$  indicates the ratio  $(\text{H}_2\text{SO}_4)_n / (\text{H}_2\text{SO}_4)_{n-1}$ . Note that the notation  $(\text{H}_2\text{SO}_4)_n$  is shorthand for the summation of  $(\text{H}_2\text{SO}_4)_n(\text{H}_2\text{O})_m$  over  $m$ .

The ratios  $R_6$  and higher are  $\sim 0.5$  which may indicate that they are determined by the ratios of the efficiency of incorporation of  $\text{H}_2\text{SO}_4$  into the successive clusters if steady state had

been attained. Then, for example,  $R_6 \sim k_{6f}/k_{7f}$  at steady state and the decomposition rate,  $k_{6r}$ , is very small. The measured ratios are consistent with an increase in  $k_{nf}$  with  $n$  due to the increase in size of the cluster with  $n$ .

It is possible that for some clusters, i.e.  $n = 3$  and perhaps 4, the measurements reflect equilibrium distributions and thus  $K_{3 \text{ or } 4}$  could be estimated. As mentioned above, the equilibrium constants are properly defined by including the hydration of reactants and products whereas our measured ratios are likely to be the sum of all hydrated clusters. Thus in comparisons of theory with these results, the predicted equilibrium constants would need to be summed over all hydrates.

Our results are in accord with one theory of bimolecular nucleation where the critical cluster size is predicted to be  $n \sim 4$  for these conditions.<sup>15</sup> In addition, this parameterization predicts that the nucleation rate is  $10^6$  to  $10^8$  particles  $\text{cm}^{-3} \text{ s}^{-1}$  for the 50 % RH conditions. Taking our observed concentration of the presumed critical cluster,  $n = 4$ ,  $\sim 10^7 \text{ cm}^{-3}$ , and multiplying by the first-order rate coefficient for the addition of an  $\text{H}_2\text{SO}_4$  molecule,  $[\text{H}_2\text{SO}_4]k_{5f}$ , we arrive at an estimate of a few times  $10^6$  particles  $\text{cm}^{-3} \text{ s}^{-1}$  for the nucleation rate. For these types of theories and these types of experiments, this agreement is remarkably quantitative.

## Conclusions

The present investigation provides new insight into the formation of molecular clusters of sulfuric acid and water. The experiments were done under temperatures and  $[\text{H}_2\text{O}]$  that are typical of the middle-to-upper troposphere as well as the high latitude, lower troposphere. Unavoidably, the sulfuric acid concentrations were one to two orders of magnitude higher than those typical of the atmosphere. The experimental technique must also be refined in order to

provide better, more quantitative results. Thus direct application to the atmosphere awaits future revision of the technique. These include better determination of the time allowed for cluster growth and the attainment of a more uniform gas temperature in the flow tube.

These laboratory measurements are used to derive rough steady-state ratios of  $\text{H}_2\text{SO}_4$  clusters that may be compared to those predicted by theories. This may be the first empirical data set against which the first steps of bimolecular nucleation theory can be tested. The results of this initial study are qualitatively in agreement with bimolecular nucleation theories<sup>4,15</sup> in that both suggest a positive correlation between cluster growth and water acid concentrations and are suggestive that the critical cluster is near  $n = 4$ . Furthermore, there is semi-quantitative agreement between the nucleation rate estimated from our measurements and predicted<sup>15</sup> nucleation rates. Note that this theory was also in good agreement with recently<sup>6</sup> measured nucleation rates at 295 K and RH = 8%. Although some disagreements between measurements and predicted nucleation rates still exist, notably the RH dependencies, it can be concluded that the refinements of the classical, liquid-drop nucleation theory for the  $\text{H}_2\text{O}$ - $\text{H}_2\text{SO}_4$  binary system has resulted in improved agreement with experiment.

We also presented evidence that the largest clusters observed, the pentamer through octamer, are probably greater than the size of a critical nucleus under the temperature and relative humidity condition of the experiment.<sup>6,15</sup> Thus, in addition to the first steps of the nucleation process, some of the growth steps may now be observable.

Another important aspect of this report is the demonstration that the non-volatile chemical details of cluster growth can be observed. Bimolecular nucleation may be responsible for only a portion of the nucleation process in the remote atmosphere<sup>1</sup> and new particle formation in urban environments is probably very removed from the simple  $\text{H}_2\text{SO}_4/\text{H}_2\text{O}$  system.

If another species is influencing particle nucleation in the atmosphere, it may be found out using this experimental technique. It is likely that molecular information during cluster growth is required if anthropogenically induced nucleation is to be understood. In addition to refining the technique, we hope to extend these studies to include other species such as ammonia which has been shown to lead to enhanced nucleation rates when added to H<sub>2</sub>SO<sub>4</sub>/H<sub>2</sub>O gas mixtures.<sup>6</sup>

### **Acknowledgments.**

We thank D. Voisin for help in various aspects of this work. Conversations with E. R. Lovejoy and P. McMurry are gratefully acknowledged. This research was in part supported by NASA grant NAG5-6383.

### **References and Notes:**

- 1) Weber, R.J., P.H. McMurry, R. L. Mauldin III, D.J. Tanner, F.L. Eisele, A.D. Clarke and V.N. Kapustin, New particle formation in the remote troposphere: A comparison at various sites *Geophys. Res. Lett.*, *26*, 307-310, 1999.
- 2) Weber, R.J., J.J. Marti, P.H. McMurry, F.L. Eisele, D.J. Tanner, and A. Jefferson Measured atmospheric new particle formation rates: Implications for nucleation mechanisms, *Chem. Eng. Comm.*, *157*, 53-64, 1996.
- 3) Coffman, D.J., and D.A. Hegg, A preliminary study of the effect of ammonia on particle nucleation in the marine boundary layer, *J. Geophys. Res.*, *100*, 7147-7160, 1995.
- 4) Jaecker-Voirol, A., and P. Mirabel, Nucleation rate in a binary mixture of sulfuric acid and water vapor, *J. Phys. Chem.*, *92*, 3518, 1988.

- 5) Laaksonen, A., V. Talanquer, D. W. Oxtoby, Nucleation: measurements, theory, and atmospheric applications, *Ann. Rev. Phys. Chem.*, *46*, 489-524, 1995.
- 6) Ball, S.M., D. R. Hanson, F. Eisele, and P. H. McMurry, Laboratory studies of particle nucleation. Initial results for H<sub>2</sub>SO<sub>4</sub>, H<sub>2</sub>O, and NH<sub>3</sub> vapors *J. Geophys. Res.*, *in press*, 1999.
- 7) Viisanen, Y., M. Kulmala, and A. Laaksonen, Experiments on gas-liquid nucleation of sulfuric acid and water *J. Chem. Phys.*, *107*, 920, 1997.
- 8) Wyslouzil, B.E., J.H. Seinfeld, R.C. Flagan, and K. Okuyama, Binary Nucleation in acid-water systems. II. Sulfuric acid-water and a comparison with methane sulfonic-water *J. Chem. Phys.*, *94*, 6842-6850, 1991.
- 9) Lovejoy, E.R. and D. R. Hanson, Kinetics and products of the reaction SO<sub>3</sub>+NH<sub>3</sub>+N<sub>2</sub>, *J. Phys. Chem.*, *100*, 4459, 1995.
- 10) Eisele, F.L., and D.J. Tanner, Measurement of the gas phase concentration of H<sub>2</sub>SO<sub>4</sub> and methane sulfonic acid and estimates of H<sub>2</sub>SO<sub>4</sub> production and loss in the atmosphere, *J. Geophys. Res.*, *98*, 9001-9010, 1993. Tanner, D.J., A. Jefferson and F.L. Eisele, Selected ion chemical ionization mass spectrometric detection of OH *J. Geophys. Res.*, *102*, 6415, 1997.
- 11) Viggiano et al., *J. Phys. Chem.*, *101*, 8270, 1997.
- 12) The ion mobility of the HSO<sub>4</sub><sup>-</sup>(H<sub>2</sub>SO<sub>4</sub>)<sub>n-1</sub> cluster is likely to be a weak function of *n*, approximately inverse square root, thus the ion drift time likely increases as  $\sim n^{1/2}$ . To a first approximation, however, it is balanced by a compensating change in  $k'_n$  with *n*: the collision rate of the ion with H<sub>2</sub>SO<sub>4</sub> molecules also depends approximately on the square root of the mass of the ion. Thus (8) is an adequate approximation for the time dependence of the *n*th ion cluster due to the ion clustering process. These facts about *t* and  $k'_n$  should be kept in mind, however, when extracting values for the rate coefficients from the data.

- 13) Several peaks attributed to impurities can be identified in Figure 2. Species giving ions at 113, 134, and 209 amu plus their clusters with HNO<sub>3</sub> and H<sub>2</sub>SO<sub>4</sub> were observed. Also, signals at ~308 and ~408 amu are noticeable. The signals due to these species were highly variable and did not noticeably affect the observations of the sulfuric acid clusters with only few exceptions (e.g., the <sup>34</sup>S isotope for the dimer at 197 amu is also the mass for the 134·HNO<sub>3</sub> ion). The isotopic ratios of the species giving the 113 amu ion were measured and are consistent with the species CF<sub>3</sub>CO<sub>2</sub><sup>-</sup>, the ion produced from reaction of NO<sub>3</sub><sup>-</sup> with trifluoroacetic acid.
- 14) A rough value for the rate coefficient k'<sub>3</sub> can be derived from the data in figure 3c assuming the trimer signal is due only to ion clustering: k'<sub>2</sub> ~ 8x10<sup>-10</sup>. Note that the data follow a t<sup>2</sup> behavior.
- 15) Kulmala, M., A. Laaksonen, and L. Pirjola, Parameterizations for sulfuric acid/water nucleation rates, *J. Geophys. Res.*, 103, 8301-8307, 1998.

**Table 1.** Estimated neutral cluster ratios.

T (K)	[H <sub>2</sub> SO <sub>4</sub> ] (cm <sup>-3</sup> )	pH <sub>2</sub> O (torr)	RH	R2 <sup>!</sup>	R3 <sup>#</sup>	R4 <sup>@</sup>	R5 <sup>*</sup>	additional clusters
236	1e9	0.11	55%	~0.01	0.4	~1	~1	R6-8 ~ 0.5
236	1.2e9	0.12	63%	~0.008	0.3	0.9	0.4	R6 ~ 0.5
236	2.4e9	0.04	20%	~0.005	0.05	0.6	1	R6 ~ 0.4
257	7e8	0.64	48%	~0.004	0.06	0.14	~3	

! Observed signal was due largely to ion molecule clustering. Thus the value was obtained by extrapolation.

# The signals for n=3 are mostly due to neutral clusters but R3 has the highly uncertain neutral dimer signal in the denominator.

@ May be close to the critical cluster for the high humidity (RH>50%) data.

\* Either there was insufficient time for steady state to be achieved or n=5 is near the critical cluster size. For example, the 257 K observed ratio is higher than that at lower temperatures. See text for discussion.

## FIGURE CAPTIONS.

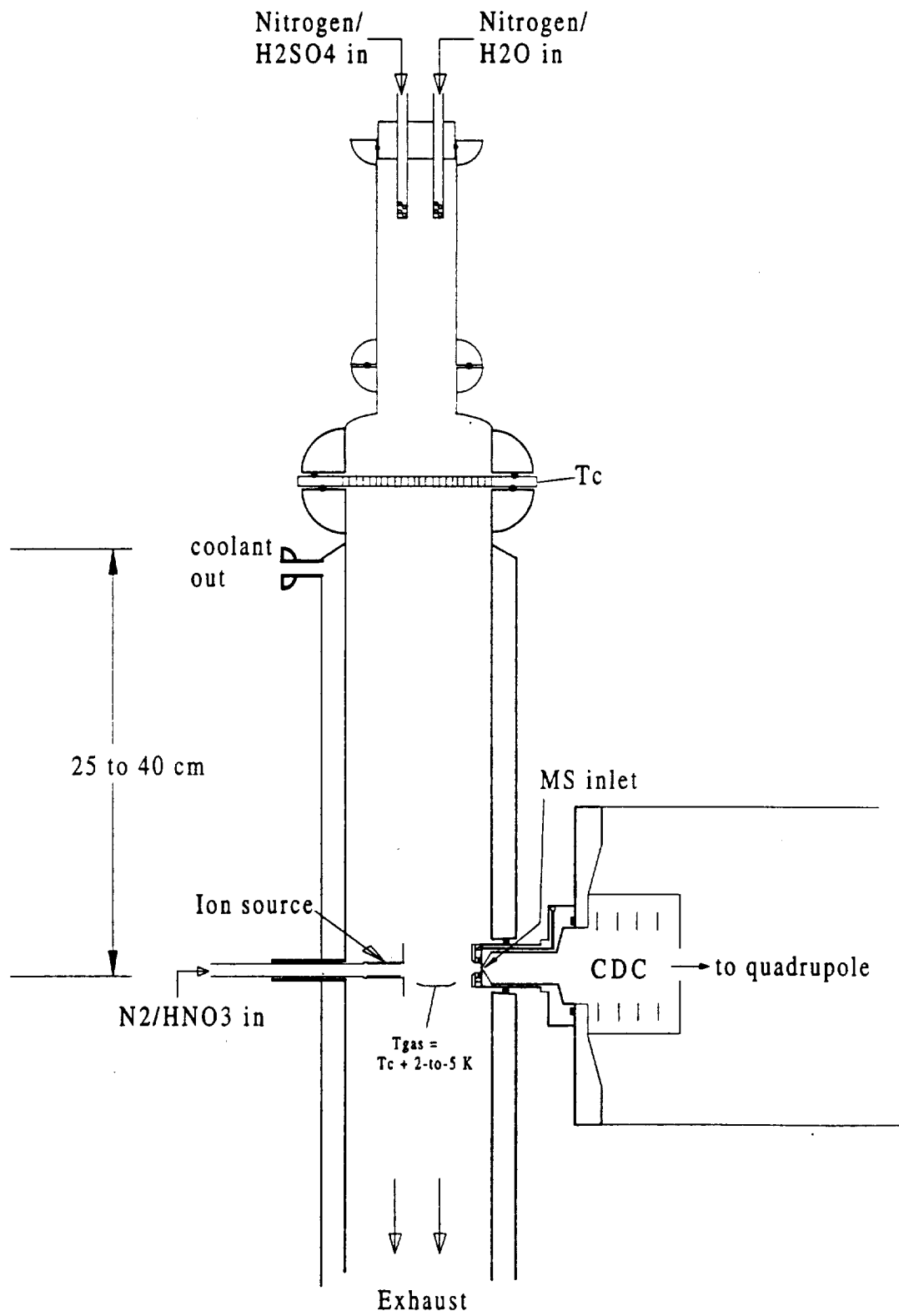
**Figure 1.** Schematic drawing of the cooled flow tube with the ion source and mass spectrometer inlet transverse to the flow. Ion reaction time is controlled by either changing the electric field or the distance between the source and inlet.

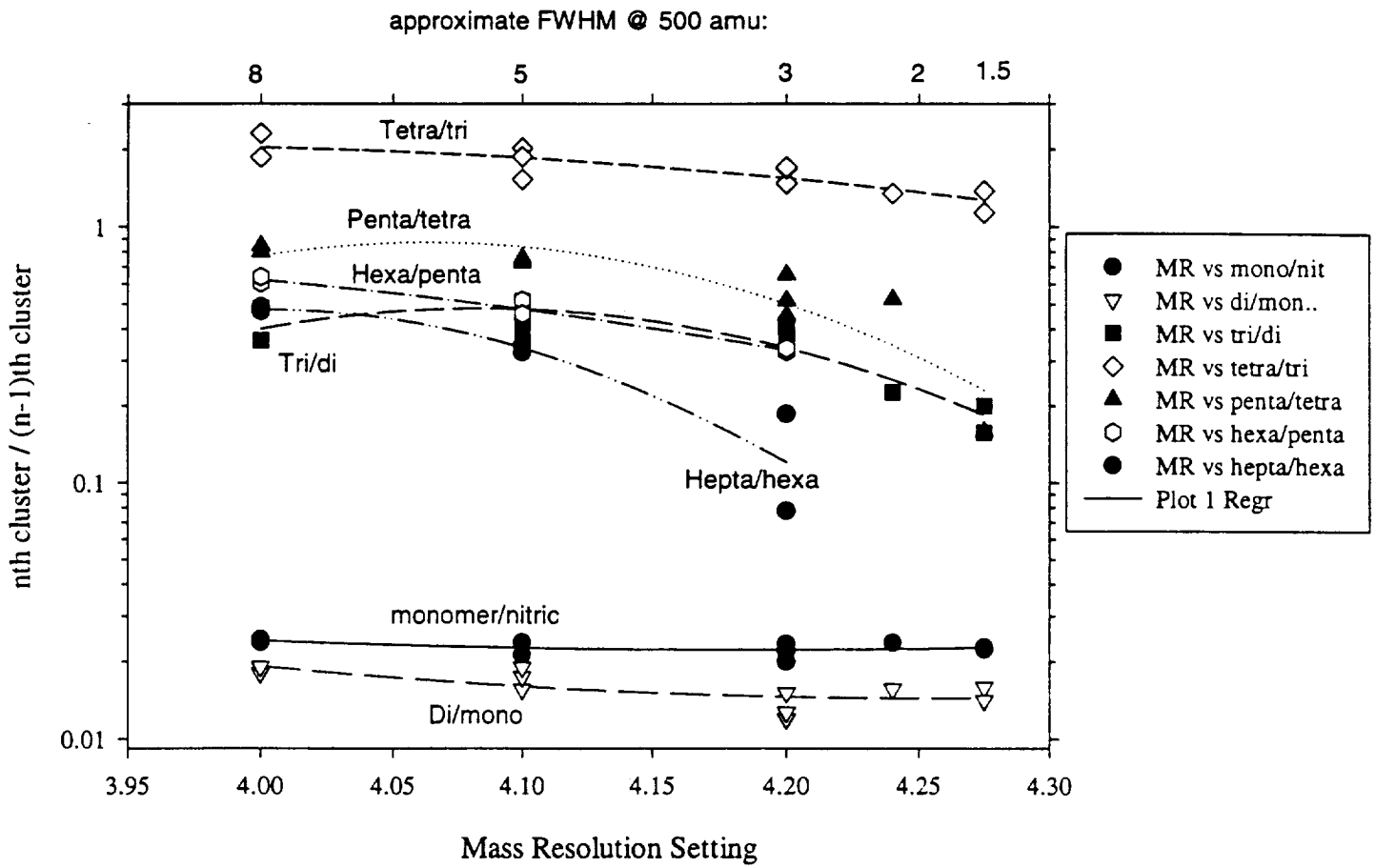
**Figure 2.** Ratios of successive clusters of  $\text{H}_2\text{SO}_4$  versus mass resolution setting. The approximate full-width at half maximum of a mass peak at  $\sim 500$  amu is indicated at the top of the figure.

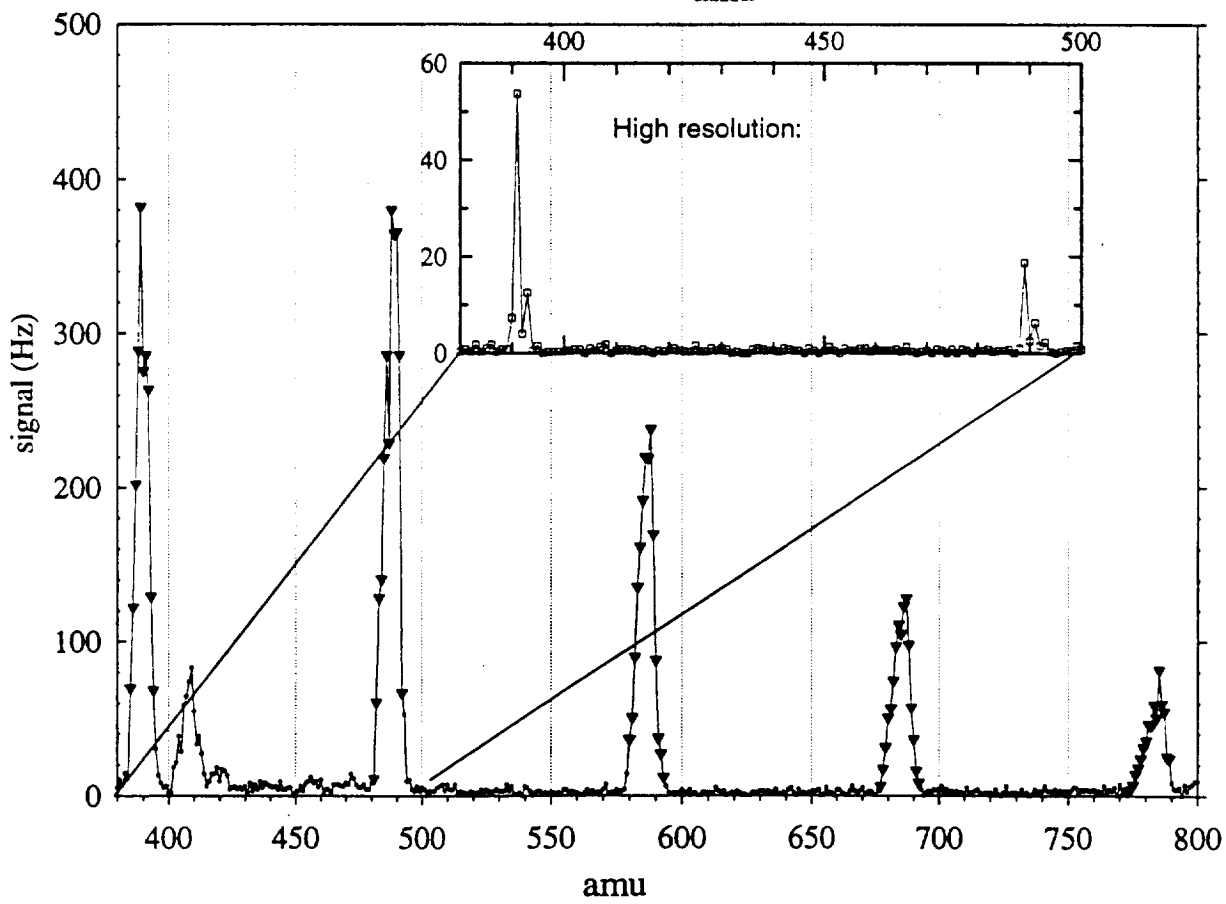
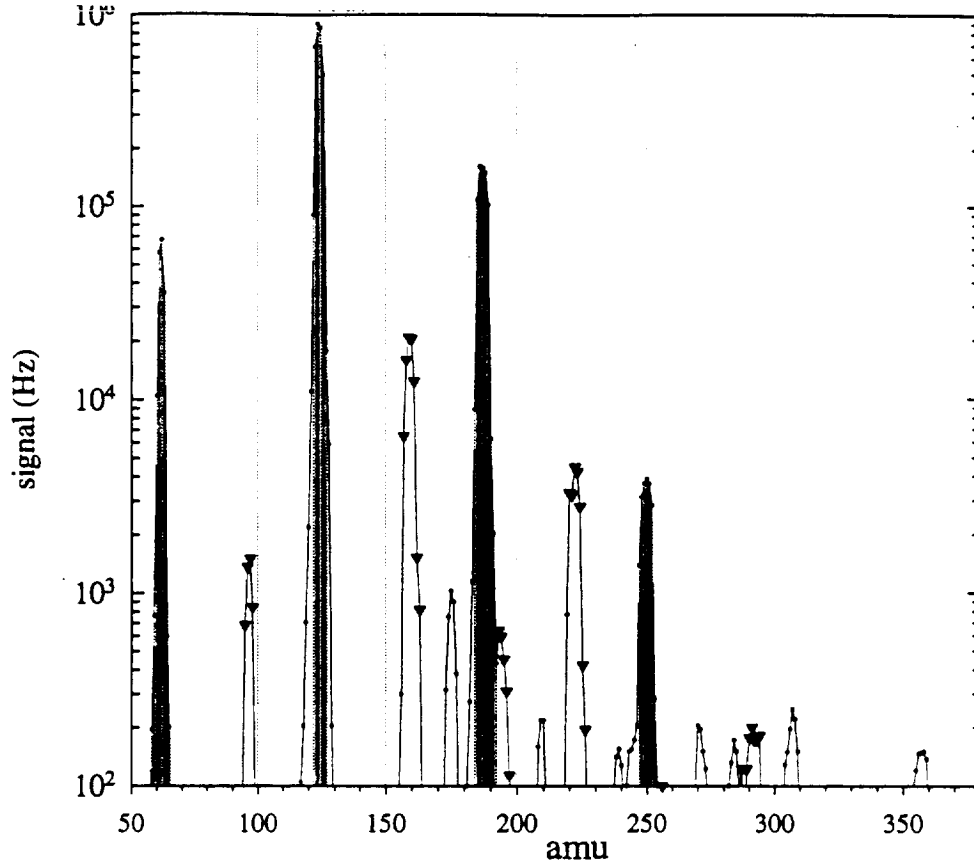
**Figure 3.** A mass spectrum at 236 K and  $\sim 60\%$  RH obtained at the low mass resolution used to calculate  $R_n$  values.  $[\text{H}_2\text{SO}_4]$  was  $\sim 1 \times 10^9 \text{ cm}^{-3}$ . The  $\text{NO}_3^-$  core ions are shaded in gray and the ions associated with  $\text{H}_2\text{SO}_4$  and its clusters are indicated by filled triangles. Note the change in logarithmic scale to linear scale at 380 amu. The inset is a higher resolution scan of the 391 and 489 amu peaks.

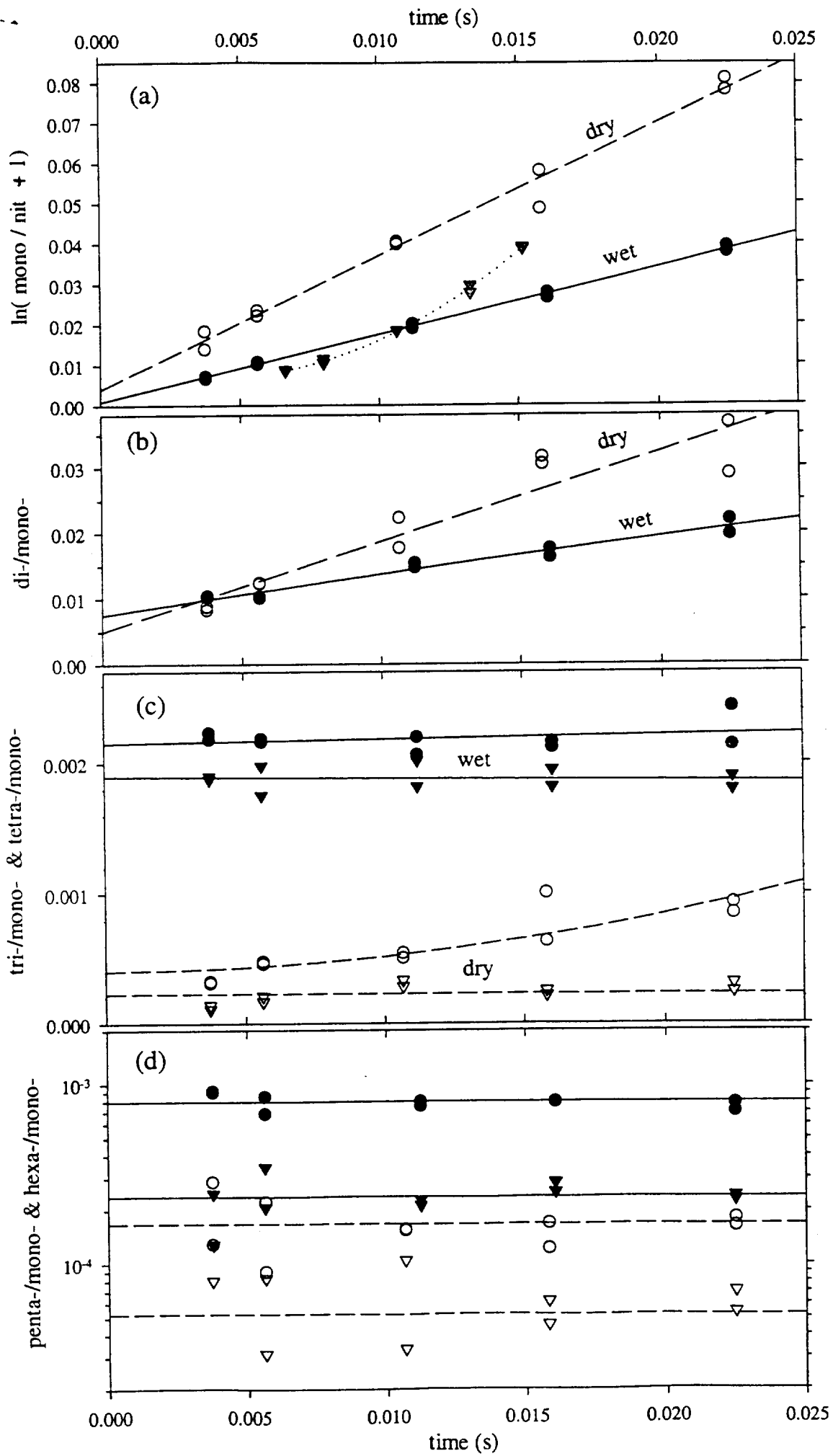
**Figure 4.** Ion ratios versus ion-molecule reaction time for two experiments at 236 K with water vapor at 0.12 torr (filled symbols, solid lines) and 0.04 torr (open symbols, dashed lines). (a) The monomer to nitric ratios are shown along with an experiment at the high RH where the source-inlet distance was changed (shaded triangles), (b) the dimer to monomer signal ratios, (c) the trimer and tetramer to monomer ratios, and (d) the pentamer and hexamer to monomer ratios are plotted on a log axis versus time.

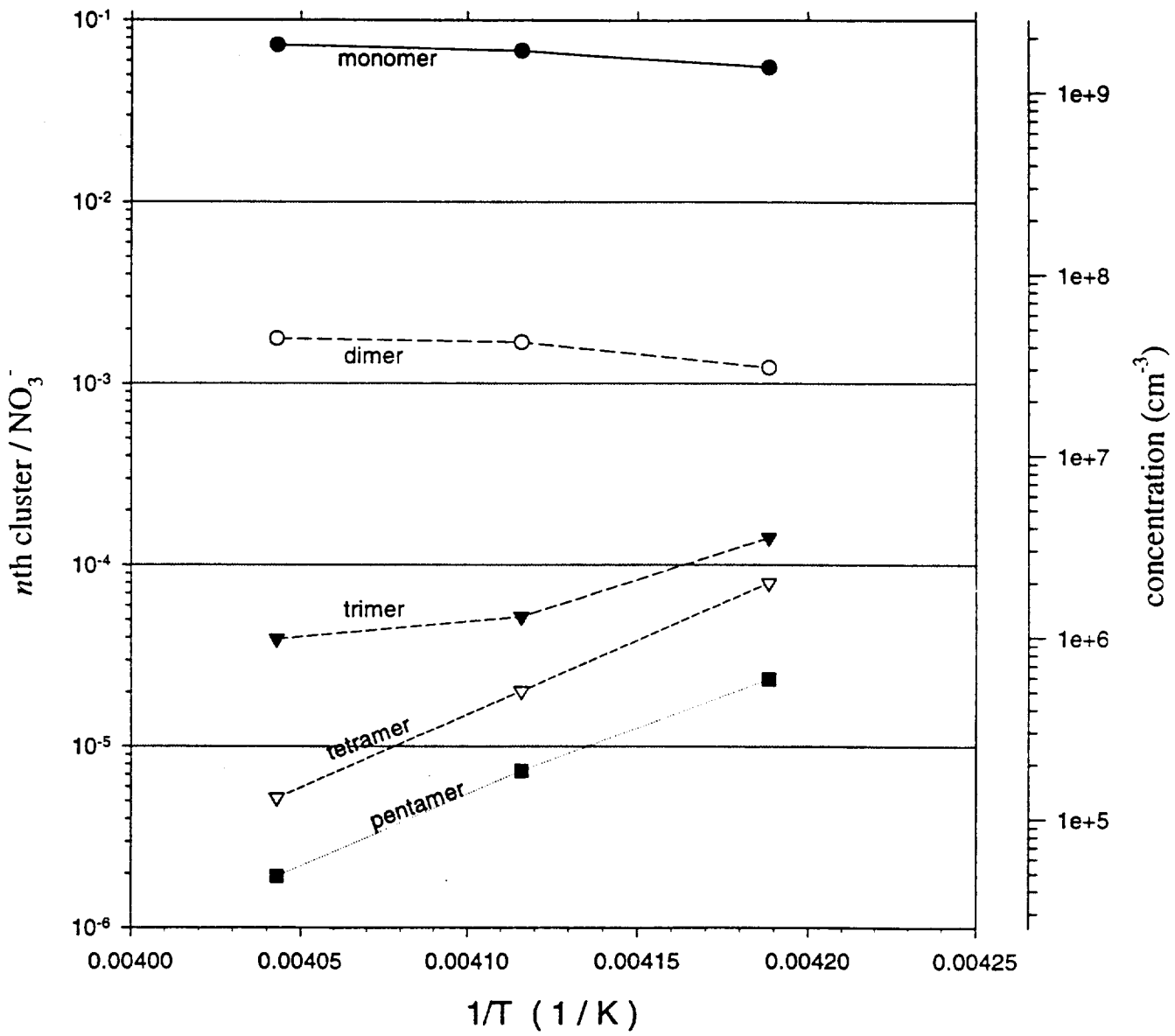
**Figure 5.** The  $\text{HSO}_4^-(\text{H}_2\text{SO}_4)_{n-1}$  cluster signals up to  $n = 5$  divided by the  $\text{NO}_3^-$  ion signals are shown as a function of inverse temperature at constant water vapor = 0.1 torr. Note the apparent stabilization of the large clusters at low temperatures.











5

Diffusion of H<sub>2</sub>SO<sub>4</sub> in humidified nitrogen: hydrated H<sub>2</sub>SO<sub>4</sub>D. R. Hanson and F. Eisele<sup>1</sup>

Atmospheric Chemistry Division, National Center for Atmospheric Research Boulder, CO

*for J. Phys. Chem.* 10-Sep-99.

**Abstract.** First-order rate coefficients for the wall loss of H<sub>2</sub>SO<sub>4</sub> were measured as a function of relative humidity in a high-pressure laminar flow tube in conjunction with chemical ionization mass spectrometry detection. The measurements yield a diffusion coefficient for H<sub>2</sub>SO<sub>4</sub> vapor in N<sub>2</sub> at 298 K of 0.094 (±0.006) atm cm<sup>2</sup> s<sup>-1</sup>. For relative humidities (RH) up to about 40 %, the measured first-order loss rates steadily decreased as the RH was increased. The effective diffusion coefficient at 40 % RH was ~20 % less than without H<sub>2</sub>O present. The measured loss rates were less dependent on water vapor for RH between 40 and 70 %. We interpret these observations as due to the addition of up to two H<sub>2</sub>O molecules to H<sub>2</sub>SO<sub>4</sub>, thus slowing the diffusion rate to the wall. The results indicate that about half the H<sub>2</sub>SO<sub>4</sub> molecules are hydrated at ~8 % RH and it is likely a second water molecule interacts with this species at higher RH. Calculations of the decrease in diffusivity of H<sub>2</sub>SO<sub>4</sub> due to addition of water are consistent with the observed decreases.

**Introduction.**

Aerosol particles in the atmosphere have potentially wide-ranging effects on climate, on atmospheric composition, and on health. Consequently, understanding their origin and growth and loss processes has been an active area of research. Field measurements [Weber et al. 1999]

---

<sup>1</sup> also School of Earth and Atmospheric Sciences, Georgia Institute of Technology, Atlanta, GA 30332

and theoretical considerations [Laaksonen et al. 1995] indicate that the  $\text{H}_2\text{SO}_4$  molecule plays a key role in these processes.

The nucleation rate of particles from  $\text{H}_2\text{SO}_4$  and  $\text{H}_2\text{O}$  vapors, according to the classical theory, depends upon the hydration of  $\text{H}_2\text{SO}_4$  vapor molecules, of which the first step is



It is likely that in other nucleating systems involving  $\text{H}_2\text{SO}_4$ , such as  $\text{NH}_3/\text{H}_2\text{SO}_4/\text{H}_2\text{O}$  or ion-induced nucleation processes, (1) will also be important. In the classical theory of nucleation, acid molecules that are hydrated do not contribute to the relative acidity (RA) and thus calculated nucleation rates decrease when  $\text{H}_2\text{SO}_4$  is hydrated. Consequently, there have been a number of studies that have derived hydrate distributions using simple models in combination with the thermodynamics of bulk solutions (classical hydrate theory, [Jaeger-Voirol and Mirabel, 1988; Kulmala et al., 1991]). At 50 % RH, for example, ~10% of  $\text{H}_2\text{SO}_4$  vapor molecules are unhydrated, ~40% are present as  $\text{H}_2\text{SO}_4 \cdot \text{H}_2\text{O}$  and ~40% are present as  $\text{H}_2\text{SO}_4 \cdot (\text{H}_2\text{O})_2$  (the balance is primarily  $\text{H}_2\text{SO}_4 \cdot (\text{H}_2\text{O})_3$ .) However, recent work has cast doubt on the classical hydrate theory. Theoretical *ab initio* calculations at the molecular level are consistent with less hydration than the classical hydrate theory suggests [Arstilla et al., 1998; Bandy and Ianni, 1998] however a molecular dynamics simulation [Kusaka et al., 1998] predicts very extensive hydration, more even than the classical theory. Furthermore, a rough comparison of measured [Marti et al., 1997] and calculated  $\text{H}_2\text{SO}_4$  vapor pressures of  $\text{H}_2\text{SO}_4/\text{H}_2\text{O}$  solutions suggests that hydrate formation is less extensive than the hydrate theory suggests [McGraw and Weber, 1998].

Reaction (1) will also be important in nucleation theories based on the thermodynamics of individual molecular clusters. Thus information regarding (1), as well as the supplementary hydration reactions, will be important for understanding the formation of atmospheric particles. We present here evidence for the hydration of  $\text{H}_2\text{SO}_4$  from measurements of the diffusion rate of  $\text{H}_2\text{SO}_4$  and  $\text{H}_2\text{SO}_4 \cdot (\text{H}_2\text{O})_n$  as a function of water partial pressure.

## EXPERIMENT.

$\text{H}_2\text{SO}_4$  loss measurements were carried out in a vertically-mounted cylindrical flow reactor (i.d. 4.9 cm  $\times$  105 cm long) held at 298 K by circulating a thermostatted liquid through a jacket surrounding the reactor.  $\text{N}_2$  gas with variable amounts of  $\text{H}_2\text{O}$  was flowed into a short (35 cm) flow tube attached to the top of the flow reactor. A flow straightener (a  $\frac{1}{2}$ " thick aluminum plate with  $\sim$  50 evenly spaced  $\frac{1}{8}$ " holes) was positioned between the flow reactor and this section to decrease perturbations to the flow due to the gas inlets above it (suppressed the influence of gas jet streams).  $\text{H}_2\text{SO}_4$  vapor was entrained in a separate flow of  $\text{N}_2$  through a movable injector and  $[\text{H}_2\text{SO}_4]$  was monitored with a selected-ion chemical ionization mass spectrometer, SICIMS [Eisele and Tanner, 1993 ; Ball et al., 1999].

The movable 'showerhead' injector is made of teflon and glass tubing and is 4 cm long  $\times$  4.85 cm in diameter (shown in Figure 1).  $\text{N}_2$  enters the injector via a long thin teflon tube which also suspended the injector vertically in the flow reactor. This flow was distributed through approximately 30 evenly spaced 0.033 cm holes. The  $\text{N}_2$  then picked up  $\text{H}_2\text{SO}_4$  vapor as it passed through glass wool that had been soaked with  $\sim$  1 g of 98 % sulfuric acid. A separate gas flow of  $\text{N}_2/\text{H}_2\text{O}$  passed through the flow straightener and traveled down the reactor and through the injector via  $\sim$  thirty evenly spaced 0.4 cm i.d. glass tubes. The  $\text{N}_2/\text{H}_2\text{SO}_4$  and  $\text{N}_2/\text{H}_2\text{O}$  flows mixed below the injector. Generally, the  $\text{N}_2/\text{H}_2\text{SO}_4$  flow was half (or less) of the total flow.

$\text{H}_2\text{SO}_4$  in the reactor effluent was detected by reaction with  $(\text{HNO}_3)_m\text{NO}_3^-$  core ions ( $m \leq 2$ ) and monitoring the product  $\text{HSO}_4^-$  ions after stripping them of  $\text{HNO}_3$  and  $\text{H}_2\text{O}$  molecules in a collisional dissociation chamber. The SICIMS is described in detail by Eisele and Tanner [1993]. Some measurements were also performed with a transverse ion source-mass spectrometer inlet scheme [Eisele and Hanson, submitted manuscript]. Typically, the initial

average  $[\text{H}_2\text{SO}_4]$  was 0.1-to- $1 \times 10^{10}$  molecule  $\text{cm}^{-3}$  although for high relative humidity measurements requiring low flows through the  $\text{H}_2\text{SO}_4$  injector it was as low as  $\sim 3 \times 10^7$   $\text{cm}^{-3}$ .

Total  $\text{N}_2$  flow in the reactor was typically 1.6 standard liter  $\text{min}^{-1}$  (slpm), temperature was 298 K, and total pressure was 620 torr resulting in an average flow speed of  $1.9 \text{ cm s}^{-1}$ . An additional flow of  $\text{N}_2$  ( $\sim 2$  slpm) was added to the reactor effluent to provide the flow required by the SICIMS (not necessary for the transverse scheme). The  $\text{H}_2\text{O}$  partial pressure was varied from  $\sim 0.1$  torr to  $\sim 16$  torr by passing a portion of the flow through a perforated teflon tube in a water bath [Ball et al., 1999].  $P_{\text{H}_2\text{O}}$  was monitored with a dew/frost point hygrometer and comparison with the flow measurements indicated the flow through the saturator was fully saturated with  $\text{H}_2\text{O}$  at its vapor pressure for  $\text{N}_2$  flows of 2 slpm and less. To check for buoyancy effects, in some experiments  $\text{O}_2$  was added to this flow to maintain a gas density equal to that of  $\text{N}_2$ . This made no difference in the results suggesting differences in buoyancy between the two gases does not lead to a significantly disturbed flow.

In separate experiments, the flow was visualized by entraining micron sized sulfuric acid particles in either the injector ( $\text{H}_2\text{SO}_4$ -containing) or the main ( $\text{H}_2\text{O}$ -containing) flows and they were illuminated with a HeNe laser. In the measurement region all particles flowed downwards for total flow rates up to  $\sim 3$  slpm; for total flows larger than this gas jets and swirling was noted in the region just below the injector. The speed of the particles was crudely measured by recording the time they took to traverse a distance of 12 cm for total flow rates of 1 and 1.5 slpm. This was done for particles on the centerline of the reactor at a distance of  $\sim 40$  cm downstream of the injector. The speed of the flow was measured to be within a few percent, well within the accuracy of the measurement, of that expected for fully developed laminar flow where the axially centered flow speed is twice the average flow.

The injector was kept a distance of at least 20 cm away from the flow straightener to minimize disturbances to the flow through the injector (this distance is greater than the 5-to-15

cm distance required for laminar flow to develop from an initial plug-type flow). Also, the distance between the injector and the end of the thermostatted measurement region (i.e., the injector position) was kept greater than the inverse of the wall loss rate coefficient (16 to 40 cm depending upon flow rate). This was done because  $[\text{H}_2\text{SO}_4]$  measured too near to the injector might be influenced by high order terms [Brown, 1978]. The measured wall loss rate coefficient (units of  $\text{cm}^{-1}$ ) times the average flow velocity results in the quantity  $k_w$ , which is the measured first-order wall loss rate coefficient ( $\text{s}^{-1}$ ).  $k_w$  as a function of total flow rate is shown in Figure 2 for 2 and 42 % RH. The measured  $k_w$  are independent of flow rate over the range 0.9 to 2.2 slpm for 2 % RH and from 0.7 to  $\sim 2$  slpm for 42 % RH. These observations provide strong evidence that the flow was characteristic of fully developed laminar flow for total  $\text{N}_2$  flow rates  $\leq 2$  slpm.

We found that the glass wall of the reactor acted as a sink for  $\text{H}_2\text{SO}_4$  so that once a  $\text{H}_2\text{SO}_4$  molecule contacted the wall it did not come back off. This was true even for RH as low as 1 % when  $[\text{H}_2\text{SO}_4]$  was comparable to the equilibrium  $\text{H}_2\text{SO}_4$  vapor concentration over a bulk solution (e.g., at 1 % RH and 298 K the vapor pressure is  $\sim 3 \times 10^9 \text{cm}^{-3}$  [Clegg et al. 1998; Marti et al. 1997]). If the wall did not act as an irreversible sink, then, after some  $\text{H}_2\text{SO}_4$  had been deposited, it should provide a measurable source of  $\text{H}_2\text{SO}_4$ . This was checked for by turning off the  $\text{N}_2$  through the  $\text{H}_2\text{SO}_4$  source. The  $\text{H}_2\text{SO}_4$  coming off the walls and entraining in the flow was small even for RH as low as 1 %, resulting in  $[\text{H}_2\text{SO}_4]_{\text{wall}} < 10^7 \text{cm}^{-3}$ , much less than the equilibrium vapor pressures would give. Note that  $[\text{H}_2\text{SO}_4]_{\text{wall}}$  was subtracted from  $[\text{H}_2\text{SO}_4]$  in the analysis as done previously by Poschl et al. Finally, loss rate coefficients did not depend upon initial  $[\text{H}_2\text{SO}_4]$ , which indicates that treating the data in this manner is correct. We conclude that the measured loss rates are equal to the diffusion-limited rates.

The wall exhibited a significant  $\text{H}_2\text{SO}_4$  partial pressure after it had been exposed to high  $[\text{H}_2\text{SO}_4]$  and also at very low RH even after a minimal exposure to  $\text{H}_2\text{SO}_4$ . After the flow reactor had been exposed to high  $[\text{H}_2\text{SO}_4]$  the wall exhibited a vapor pressure that was close to

the equilibrium vapor pressure over bulk solutions [Clegg et al. 1998] (e.g.,  $[\text{H}_2\text{SO}_4]$  was  $\sim 1 \times 10^{11} \text{ cm}^{-3}$  during particle nucleation experiments [Ball et al., 1999] conducted in the same flow reactor). Rinsing the wall with de-ionized water eliminated this source and restored it to acting as a sink. At very low RH ( $\sim 0.1\%$ ) and with a relatively clean wall,  $[\text{H}_2\text{SO}_4]_{\text{wall}}$  was  $\sim 3 \times 10^8 \text{ cm}^{-3}$ , which is much less than the vapor pressure would give ( $\sim 3 \times 10^{10} \text{ cm}^{-3}$ ) but is comparable to the  $[\text{H}_2\text{SO}_4]$  coming from the injector. These data were not used to extract diffusion coefficients because it is not known if  $[\text{H}_2\text{SO}_4]_{\text{wall}}$  is a function of axial distance. If  $[\text{H}_2\text{SO}_4]_{\text{wall}}$  varies along the length of the reactor and it is a significant fraction of  $[\text{H}_2\text{SO}_4]$ , then the measured first-order loss rates will not be simply related to the diffusion coefficient. Therefore, the measurements where  $[\text{H}_2\text{SO}_4]_{\text{wall}}$  was  $> 20\%$  of  $[\text{H}_2\text{SO}_4]_0$  (i.e., greater than  $\sim 10^8 \text{ cm}^{-3}$ ) were not included. This effectively limited the RH to greater than  $\sim 0.35\%$ .

For diffusion limited wall loss of a species with diffusion coefficient  $D_c$  in a cylindrical flow tube of radius  $r$ , the first-order rate coefficient  $k_{\text{dl}} (\text{s}^{-1})$  is given by

$$k_{\text{dl}} = 3.65 D_c / r^2 \quad 2$$

The measured  $k_w$  are set equal to  $k_{\text{dl}}$  whereupon  $D_c$  is obtained. This equation was obtained from the treatment of Brown [1978] for diffusion in laminar flow within a cylindrical reactor. It is a shortcut valid when axial diffusion can be neglected as is the case here. The factor 3.65 is not sensitive (less than 0.3 % change) to the experimental conditions here for flow rates from 1 to 2.5 slpm. However, as the flow rate and thus axial velocity decreases further, axial diffusion becomes non-negligible and the factor 3.65 is no longer valid (e.g., at 0.5 slpm, R2 is  $\sim 2\%$  high).

The main contributions to the uncertainty in the loss rate measurements are the accuracy of the flow meter calibrations ( $\pm 2\%$ ) and the possible uncertainty in relating the loss measurement to a diffusion coefficient due to the flow not perfectly attaining laminar flow conditions. The latter should depend upon total flow rate however as discussed above the

measured  $k_w$  did not noticeably depend on flow rate. From the scatter in the  $k_w$  vs. total flow rate data depicted in Fig. 2 we estimate this latter error is  $\leq 3\%$  for measurements at low RH and  $\leq 5\%$  for measurements at high RH.

## RESULTS.

Shown in Figure 3 is  $\ln[\text{H}_2\text{SO}_4]$  vs. injector position for five measurements with RH between 0.35 and 42 %. A noticeable decrease in the wall-loss rate coefficient as  $[\text{H}_2\text{O}]$  increases is exhibited. From these loss rate coefficients, values for the diffusion coefficient of the  $\text{H}_2\text{SO}_4$  species were obtained using (2). These were divided by the total pressure to obtain the pressure independent diffusion coefficient ( $pD$ ) and these are plotted in Figure 4 as a function of RH. Note that the partial pressure of  $\text{H}_2\text{O}$  is  $\leq 2.5\%$  of the total pressure thus we can assume that  $\text{H}_2\text{SO}_4$  diffusion through an  $\text{N}_2$ - $\text{H}_2\text{O}$  (and, when present,  $\text{O}_2$ ) mixture is equivalent to that through  $\text{N}_2$  at the same total pressure.

The SICIMS measures the sum of all  $\text{H}_2\text{SO}_4$  species and thus the measured first order loss rates were set equal to an 'effective' diffusion coefficient:  $pD_{\text{eff}}$  is equal to  $P_{\text{tot}} \times D_c$  from (2). If we assume that  $\text{H}_2\text{SO}_4$  can be hydrated by up to two water molecules, the effective diffusion coefficient for the sum of the species  $\text{H}_2\text{SO}_4 \cdot (\text{H}_2\text{O})_n$  for  $n = 0$  to 2 is given by

$$pD_{\text{eff}} = \frac{pD_0 + pD_1 K_1 RH + pD_2 K_1 K_2 RH^2}{1 + K_1 RH + K_1 K_2 RH^2} \quad (3)$$

where  $pD_0$  is the diffusion coefficient of  $\text{H}_2\text{SO}_4$  in  $\text{N}_2$ ,  $pD_1$  is that for  $\text{H}_2\text{SO}_4 \cdot \text{H}_2\text{O}$ ,  $pD_2$  is that for  $\text{H}_2\text{SO}_4 \cdot (\text{H}_2\text{O})_2$ , and  $K_1$  and  $K_2$  are equilibrium constants for successive addition of  $\text{H}_2\text{O}$ . This equation is based in part on the reasonable assumption that the forward and backward rates of hydration, e.g., (1), are much faster than the diffusion transport processes. Eqn. (3) can be extended to include the cases of additional hydration steps by adding the terms  $pD_n K_1 K_2 \dots K_n (\text{RH})^n$  to the numerator and the terms  $K_1 K_2 \dots K_n (\text{RH})^n$  to the denominator.

Also shown in figure 4 is a fit to the data according to (3) (solid line). The values of the diffusion coefficients for the one and two hydrates were constrained to be 85 and 76% of the neat  $\text{H}_2\text{SO}_4$  molecule, respectively. How these constraining values were obtained is discussed below. Constraining the diffusion coefficients was done in part because allowing them to vary independently resulted in nonsensical values, i.e., that  $pD_2 \sim pD_1$ . Values for the parameters obtained from the fit are:

$$\begin{aligned}
 pD_0 &= 0.094 \pm 0.0012 \\
 K_1 &= 0.13 \pm 0.06 \\
 K_2 &= 0.016 \pm 0.006
 \end{aligned}
 \tag{4}$$

The fit to (3) is a good representation of the data and we believe the inclusion of more parameters is not warranted (errors are the  $2\text{-}\sigma$  standard deviations in the parameters). The  $2\text{-}\sigma$  precision of the measurements is  $\sim 2\%$  with a total estimated uncertainty (possible systematic +  $2\sigma$  precision) of  $\sim \pm 7\%$  for  $pD_0$ . Note the values for  $pD_1$  and  $pD_2$  were set equal to  $pD_0$  times 0.85 and 0.76, respectively, and uncertainties in these values are difficult to assign. The equilibrium constants in (3) and (4) are not in standard thermodynamic units. Using the standard state of one atmosphere to calculate activities, the standard values, denoted by  $K_1^0$  and  $K_2^0$ , are 410 and 50, respectively.

## DISCUSSION.

There are two previously reported values for the diffusion coefficient of  $\text{H}_2\text{SO}_4$  in  $\text{N}_2$  based on measurements. Lovejoy and Hanson [1996] report a value of  $0.11 \text{ atm cm}^2 \text{ s}^{-1}$  ( $\pm 20\%$ ) at 295 K and Poschl et al. [1998] report  $0.088$  ( $\pm 2\%$ ) at 303 K. Both are in agreement with the value for  $pD_0$  at 298 K reported here of  $0.094$  ( $\pm 7\%$ ) although consideration of the temperature differences deteriorates this agreement (the diffusion coefficient goes as  $\sim T^{1.75}$  [Monchick and Mason, 1961]). The observation reported by Lovejoy et al. [1996] that the measured first-order

wall loss rate coefficients for  $\text{H}_2\text{SO}_4$  at high RH was significantly less than that measured at low RH is consistent with our results.

The diffusion coefficient can be calculated assuming an interaction potential between the molecules. The most commonly used potentials are the Lennard-Jones 12-6 potential and for interactions between polar molecules, the Stockmayer (12-6-3) potential. The values for the molecular diameter and well-depth ( $\epsilon$ ) for the  $\text{H}_2\text{SO}_4$  molecule are not known. Here, we take the well depth to be  $1.35kT_b$  where  $k$  is Boltzmann's constant and  $T_b$  is the boiling point [Ayers et al. 1980]. The factor 1.35 was chosen because that gives the relation between the boiling point and the recommended well depth for  $\text{H}_2\text{O}$  [Mason and Monchick, 1962]. With this well depth for  $\text{H}_2\text{SO}_4$ ,  $\epsilon/k = 840$  K, a molecular diameter of  $4.4 \text{ \AA}$  for  $\text{H}_2\text{SO}_4$  is necessary to obtain a calculated diffusion coefficient of  $\text{H}_2\text{SO}_4$  in  $\text{N}_2$  equal to the measured value ( $0.094 \text{ atm cm}^2 \text{ s}^{-1}$ ). Also, a value of  $0.07 \text{ atm cm}^2 \text{ s}^{-1}$  for diffusion of neat  $\text{H}_2\text{SO}_4$  in  $\text{H}_2\text{O}$  vapor was calculated using these molecular parameters and a  $\delta$  parameter of 1.2 [Mason and Monchick, 1962], i.e., equal to that of the  $\text{H}_2\text{O}$ - $\text{H}_2\text{O}$  dipole interaction. The diffusion coefficients of  $\text{H}_2\text{SO}_4$  in  $\text{N}_2$  and in  $\text{H}_2\text{O}$  are similar, supporting the assumption that the small amounts of water vapor in the gas mixture can be taken to be equivalent to  $\text{N}_2$ .

An alternative approach was used to estimate the diffusion coefficients for the hydrated  $\text{H}_2\text{SO}_4$  molecules. The interaction of  $\text{N}_2$  with the  $\text{H}_2\text{SO}_4(\text{H}_2\text{O})_n$  species ( $n=0,1,2$ ) were estimated by assuming a hard sphere collision and averaging over all orientations. The atomic positions in the  $\text{H}_2\text{SO}_4(\text{H}_2\text{O})_n$  molecules were taken from recent *ab initio* theory calculations (R. Bianco, private communication; Arstilla et al. [1998]; Bandy and Ianni [1998]). The atoms were assumed to be hard-sphere like and their radii were set equal to atomic Van der Waals radii [Weast, 1983]. The  $\text{N}_2$  molecule was also approximated as a sphere. The diffusion coefficient obtained from this hard-sphere approximation for neat  $\text{H}_2\text{SO}_4$  in  $\text{N}_2$  is  $0.14 \text{ atm cm}^2 \text{ s}^{-1}$ . The ballpark agreement of this calculation with the measured values indicates this is a reasonable

approach to estimating the diffusion coefficient. The average cross section for the  $\text{H}_2\text{SO}_4\cdot\text{H}_2\text{O}$  molecule was 15 % greater than for  $\text{N}_2$  colliding with the neat  $\text{H}_2\text{SO}_4$  molecule and that for the  $\text{H}_2\text{SO}_4(\text{H}_2\text{O})_2$  species was ~ 27 % greater than that for neat  $\text{H}_2\text{SO}_4$ . Including the increases in the reduced masses, the diffusion coefficients for the first and second hydrates would be 0.85 and 0.76 times, respectively, that for the  $\text{H}_2\text{SO}_4$  molecule. As the measurements suggest a decrease in the diffusion coefficient at high RH to 0.8 times that at low RH, a slightly larger decrease than if only one water molecule is hydrating  $\text{H}_2\text{SO}_4$ . Note that this conclusion and the values of  $K_1$  and  $K_2$  depend upon the values chosen for  $pD_1/pD_0$  and  $pD_2/pD_0$ .

An alternative fit to the data using the equilibrium constants predicted from classical hydrate theory [Jaeger-Voirol and Mirabel, 1989] is shown as the dashed line in figure 4. In this theory,  $K^0_1 = 1400$  and  $K^0_2 = 55$ . The third hydration step was also included ( $K^0_3 = 14$ .) Again, the ratios of the diffusion coefficients were constrained as above along with  $pD_3$  being 68 % of the unhydrated molecule. This fit describes the data almost as well as that described above with the notable exception of the low RH region. The classical theory appears to predict hydration by a single water molecule much earlier than our data suggests. Finally, we added a third hydration step to (3) with the diffusion coefficients constrained as above and allowing the equilibrium constants to vary. The  $K_1$  and  $K_2$  did not significantly change from those in (4) and the fit value for  $K^0_3$  was 0. The 2- $\sigma$  upper limit to  $K^0_3$  was 30 ( $K_3 \leq 0.01$ ). Although the scatter in the data does not allow for drawing firm conclusions concerning the third water of hydration, the data is not inconsistent with the classical theory.

The natural logarithm of  $K^0_n$  is related to the standard free energy change of R1:

$$\ln K^0_n = -\Delta G^0_n/RT \quad (5)$$

resulting in values for  $\Delta G^0_n$  at 298 K of  $-3.6 (\pm 1)$  and  $-2.3 (\pm 0.3)$  kcal mol<sup>-1</sup> from (4), the errors are related to twice the 1 $\sigma$  errors in  $K$ . From *ab initio* calculations, Bandy and Ianni [1998] report values of  $-0.6$  and  $0$  kcal mol<sup>-1</sup> for the first and second hydration steps, respectively,

resulting in values for  $K_1^0$  of 3 and  $K_2^0$  of 1. These values result in essentially no hydration over the entire range of RH in our experiments and thus would predict virtually no change in diffusion rates as the RH is varied (e.g., at 70 % RH, a  $K_1^0$  of 3 results in hydration of ~6 % of  $\text{H}_2\text{SO}_4$  molecules.) The *ab initio* calculations of Arstilla et al. [1998] are consistent with Bandy and Ianni in that they predict enthalpies of hydration that are 3-to-5 kcal mol<sup>-1</sup> less exothermic than the classical theory of hydration predictions.

A molecular dynamics simulation of  $\text{H}_2\text{SO}_4$ - $\text{H}_2\text{O}$  clusters predicts that a  $\text{H}_2\text{SO}_4$  molecule will be extensively hydrated over the entire range of RH that we investigated [Kusaka et al. 1998]. For example, at 298 K and 39 % RH, this work predicts that the dominant cluster will be  $\text{H}_2\text{SO}_4(\text{H}_2\text{O})_4$ . Their results, however, were very dependent on their choice of the interaction parameters between  $\text{H}_2\text{SO}_4$  and  $\text{H}_2\text{O}$ . They also pointed out the sensitivity of the results to the hydration energy; differences in the latter quantity of ~1 kcal mol<sup>-1</sup> resulted in large changes in predicted hydration.

It can be concluded that the results presented here are in better agreement with the predictions of the classical hydrate theory than the predictions from the current approaches at the molecular level. It is likely that molecular level theories will need to predict the energies of the hydrates to accuracies of better than  $\pm 1$  kcal mol<sup>-1</sup> to correctly describe hydrate distributions. While disagreement over the first water of hydration is evident, the close agreement of our results with the classical predictions as regard to the second water of hydration may indicate that the classical model improves as the size of the cluster increases.

McGraw and Weber [1998] showed that measured total  $[\text{H}_2\text{SO}_4]$  over sulfuric acid aerosol [Marti et al., 1997] was not in agreement with a calculated total  $[\text{H}_2\text{SO}_4]$  using hydrate theory and theoretical neat  $\text{H}_2\text{SO}_4$  vapor pressures of the bulk solutions [Clegg et al. 1998]. The experimental study of Marti et al. was constrained to RH less than 25 % thus this rough comparison was dominated by the first water of hydration (from our results, the concentration of

$\text{H}_2\text{SO}_4(\text{H}_2\text{O})_2$  contributes only 20 % to the total  $\text{H}_2\text{SO}_4$  in the vapor at 25 % RH.) Their assertion that the liquid hydrate model overpredicts the extent of hydration pertains primarily to the addition of the first water of hydration and thus our results are in agreement with their assertion.

Nucleation events in the atmosphere that can be attributed to the  $\text{H}_2\text{SO}_4/\text{H}_2\text{O}$  binary system are likely to occur at high RH (> 50 % RH [Clarke et al., 1999]). At high RH, the presence of the  $\text{H}_2\text{SO}_4$  monohydrate may become less important than the presence of the higher hydrates which we have shown may be somewhat-accurately predicted by the classical theory. Therefore the partial success of the classical theory in explaining particle production at high RH is consistent with the notion that these theories may become more accurate as the size of the cluster increases.

### **Acknowledgments.**

Conversations with R. Bianco and E. R. Lovejoy are gratefully acknowledged. This research was in part supported by NASA grant NAG5-6383.

### **References**

- Arstila, H., K. Laasonen, and A. Laaksonen *Ab initio* study of gas-phase sulphuric acid hydrates containing 1 to 3 water molecules, *J. Chem. Phys.*, 108, 1998.
- Ayers, G.P., R.W. Gillett, and J.L. Gras, On the vapor pressure of sulfuric acid, *Geophys. Res. Lett.*, 7, 433-436, 1980.
- Ball, S.M., D. R. Hanson, F. Eisele, and P. M. McMurry, Laboratory studies of particle nucleation. Initial results for  $\text{H}_2\text{SO}_4$ ,  $\text{H}_2\text{O}$ , and  $\text{NH}_3$  vapors *J. Geophys. Res.*, *in press*, 1999.
- Brown, R.L. Kinetics of tubular flow reactors *J. Res. Natl. Bur. Stand. (U.S.)* 83, 1, 1978.
- Clarke et al. Particle production near Marine Clouds: sulfuric acid and predictions from classical binary nucleation, *Geophys. Res. Lett.*, 26, 2425, 1999.

- Clegg, S. L., P. Brimblecombe and A.S. Wexler, A thermodynamic model of the system H-NH<sub>4</sub>-SO<sub>4</sub>-NO<sub>3</sub>-H<sub>2</sub>O at tropospheric temperatures *J. Phys. Chem.*, *102A*, 2137-2154, 1998.  
(<http://www.uea.ac.uk/~e770/aim.html>).
- Eisele, F.L., and D.J. Tanner, Measurement of the gas phase concentration of H<sub>2</sub>SO<sub>4</sub> and methane sulfonic acid and estimates of H<sub>2</sub>SO<sub>4</sub> production and loss in the atmosphere, *J. Geophys. Res.*, *98*, 9001-9010, 1993.
- Jaeger-Voirol, A., and P. Mirabel, Nucleation rate in a binary mixture of sulfuric acid and water vapor, *J. Phys. Chem.*, *92*, 3518, 1988.
- Jaeger-Voirol, A., and P. Mirabel, Heteromolecular nucleation rate in the sulfuric acid-water system, *Atmos. Env.*, *23*, 2053, 1989.
- Kulmala, M., M. Lazardis, A. Laaksonen, and T. Vesala, Extended hydrates interaction model: Hydrate formation and the energetics of binary homogeneous nucleation, *J. Chem. Phys.*, *94*, 7411, 1991.
- Kusaka, I, Z.-G. Wang and J.H. Seinfeld, Binary nucleation of sulfuric acid-water: Monte-Carlo simulation, *J. Chem. Phys.*, *108*, 6829-6848, 1998.
- Laaksonen, A., V. Talanquer, D. W. Oxtoby, Nucleation: measurements, theory, and atmospheric applications, *Ann. Rev. Phys. Chem.*, *46*, 489-524, 1995.
- Lovejoy, E.R., D. R. Hanson, Kinetics and products of the reaction SO<sub>3</sub> + NH<sub>3</sub> + N<sub>2</sub> *J. Phys. Chem.*, *100*, 4459, 1996.
- Lovejoy, E.R., L.G. Huey and D. R. Hanson, Kinetics and products of the gas-phase reaction of SO<sub>3</sub> with water *J. Phys. Chem.*, *100*, 19911, 1996.
- McGraw, R., and R. J. Weber, Hydrates in binary sulfuric acid-water vapor: Comparison of CIMS measurements with the liquid drop model, *Geophys. Res. Lett.*, *25*, 1998.
- Marti, J. J., A. Jefferson, X. P. Cai, C. Richert, P. H. McMurry, and F. Eisele, H<sub>2</sub>SO<sub>4</sub> vapor pressure of sulfuric acid and ammonium sulfate solutions, *J. Geophys. Res.*, *102*, 3725-3735, 1997.

Mason, E.A. and L. Monchick, Transport Properties of Polar-Gas Mixtures, *J. Chem. Phys.*, *36*, 2746, 1962.

Monchick, L. and E. A., Mason Transport Properties of Polar Gases, *J. Chem. Phys.*, *35*, 1676, 1961.

Poschl, U. et al., Mass accommodation coefficient of H<sub>2</sub>SO<sub>4</sub> vapor on aqueous sulfuric acid surfaces and gaseous diffusion coefficient of H<sub>2</sub>SO<sub>4</sub> in N<sub>2</sub>/H<sub>2</sub>O *J. Phys. Chem. A*, *102*, 10082, 1998.

Weast, R.C., editor, Handbook of Chemistry and Physics (Chemical Rubber, Cleveland, 1983.)

Weber, R.J., P.H. McMurry, R. L. Mauldin III, D.J. Tanner, F.L. Eisele, A.D. Clarke and V.N. Kapustin, New particle formation in the remote troposphere: A comparison at various sites *Geophys. Res. Lett.*, *26*, 307-310, 1999.

**Figure 1.** Detailed cross sectional and top views of injector.

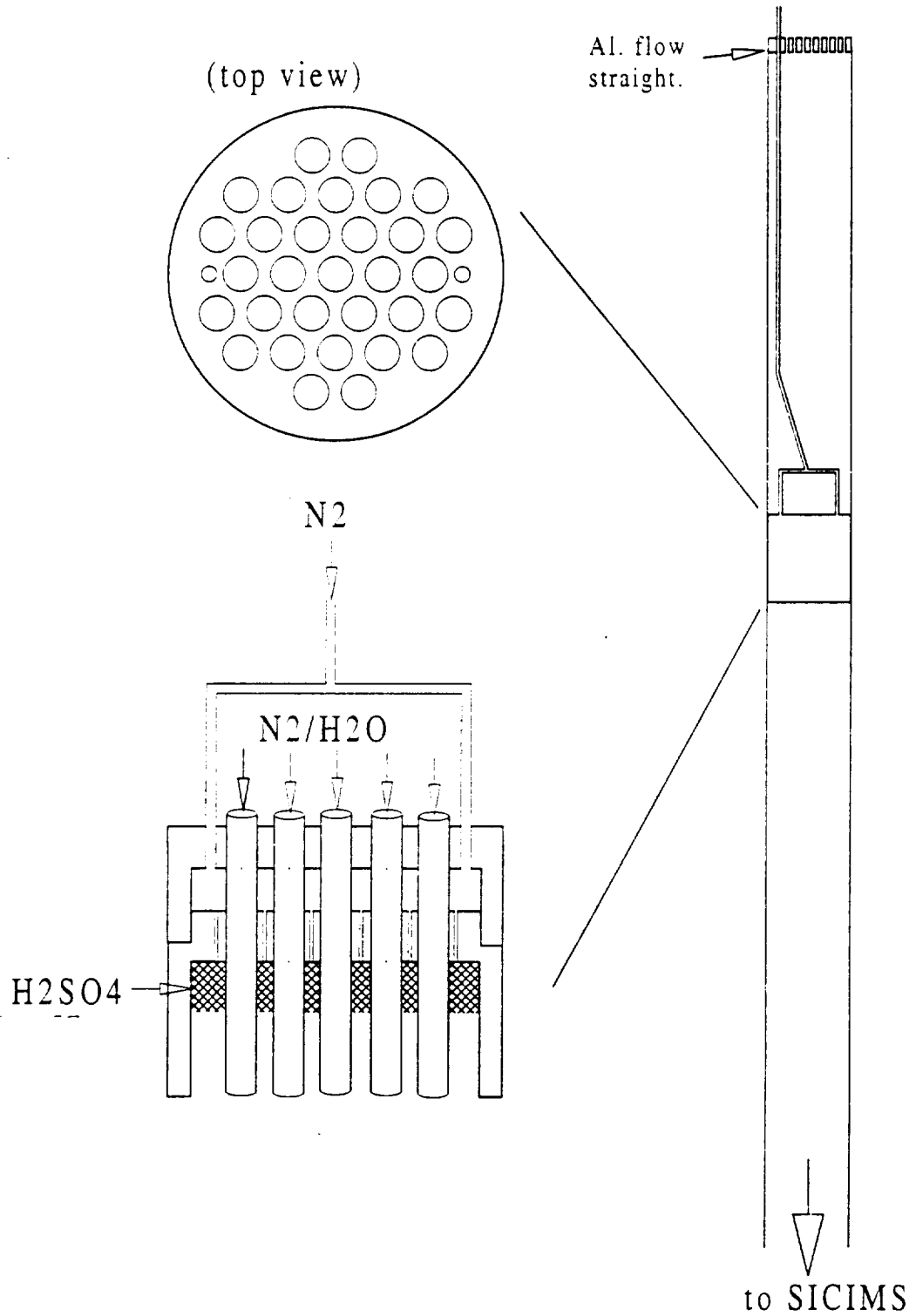
**Figure 2.** Measured wall loss rate coefficient versus total N<sub>2</sub> flow rate for 2 % and 42 % RH.

**Figure 3.** ln([H<sub>2</sub>SO<sub>4</sub>]) versus injector position for five different RH (the y-axis data for 0.35% RH was multiplied by 0.5). N<sub>2</sub> flow rate was 1.53 slpm. The loss rate coefficients for 0.35, 10, and 42 % RH are indicated in the figure.

**Figure 4.** The effective diffusion coefficient vs. RH for the species H<sub>2</sub>SO<sub>4</sub> + H<sub>2</sub>SO<sub>4</sub>·H<sub>2</sub>O + H<sub>2</sub>SO<sub>4</sub>·(H<sub>2</sub>O)<sub>2</sub> in N<sub>2</sub>. Solid and dashed lines are fits to the data according to (3) (solid: variable K<sub>1</sub> and K<sub>2</sub>; dashed: K<sub>1</sub>, K<sub>2</sub> and K<sub>3</sub> predicted by classical hydrate theory). Inset: detailed view of the low RH data.

Injector:

Flow tube



Loss rate vs. total flow: 2% and 42 % r.h.

